Anatomic, Intrinsic, and Synaptic Properties of Dorsal and Ventral Division Neurons in Rat Medial Geniculate Body

EDWARD L. BARTLETT AND PHILIP H. SMITH
Department of Anatomy and The Neuroscience Training Program, University of Wisconsin, Madison, Wisconsin 53706-1532

Bartlett, Edward L. and Philip H. Smith. Anatomic, intrinsic, and synaptic properties of dorsal and ventral division neurons in rat medial geniculate body. *J. Neurophysiol.* 81: 1999–2016, 1999. Presently little is known about what basic synaptic and cellular mechanisms are employed by thalamocortical neurons in the two main divisions of the auditory thalamus to elicit their distinct responses to sound. Using intracellular recording and labeling methods, we characterized anatomic features, membrane properties, and synaptic inputs of thalamocortical neurons in the dorsal (MGD) and ventral (MGV) divisions in brain slices of rat medial geniculate body. Quantitative analysis of dendritic morphology demonstrated that tufted neurons in both divisions had shorter dendrites, smaller dendritic tree areas, more profuse branching, and a greater dendritic polarization compared with stellate neurons, which were only found in MGD. Tufted neuron dendritic polarization was not as strong or consistent as earlier Golgi studies suggested. MGV and MGD cells had similar intrinsic properties except for an increased prevalence of a depolarizing sag potential in MGV neurons. The sag was the only intrinsic property correlated with cell morphology, seen only in tufted neurons in either division. Many MGV and MGD neurons received excitatory and inhibitory inferior colliculus (IC) inputs (designated IN/EX or EX/IN depending on excitation/inhibition sequence). However, a significant number only received excitatory inputs (EX/O) and a few only inhibitory (IN/O). Both MGV and MGD cells displayed similar proportions of response combinations, but suprathreshold EX/O responses only were observed in tufted neurons. Excitatory and inhibitory postsynaptic potentials (EPSPs and IPSPs) had multiple distinguishable amplitude levels implying convergence. Excitatory inputs activated α-amino-3-hydroxy-5-methyl-4-isoxazolepropionic acid (AMPA) and *N*-methyl-D-aspartate (NMDA) receptors the relative contributions of which were variable. For IN/EX cells with suprathreshold inputs, first-spike timing was independent of membrane potential unlike that of EX/O cells. Stimulation of corticothalamic (CT) and thalamic reticular nucleus (TRN) axons evoked a $GABA_A$ IPSP, EPSP, $GABA_B$ IPSP sequence in most neurons with both morphologies in both divisions. TRN IPSPs and CT EPSPs were graded in amplitude, again suggesting convergence. CT inputs activated AMPA and NMDA receptors. The NMDA component of both IC and CT inputs had an unusual voltage dependence with a detectable DL-2-amino-5-phosphonovaleric acid-sensitive component even below −70 mV. First-spike latencies of CT evoked action potentials were sensitive to membrane potential regardless of whether the TRN IPSP was present. Overall, our in vitro data indicate that reported regional differences in the in vivo responses of MGV and MGD cells to auditory stimuli are not well correlated with major differences in intrinsic membrane features or synaptic responses between cell types.

The costs of publication of this article were defrayed in part by the payment of page charges. The article must therefore be hereby marked ''*advertisement*'' in accordance with 18 U.S.C. Section 1734 solely to indicate this fact.

INTRODUCTION

A set of auditory thalamic nuclei, known collectively as the medial geniculate body (MGB), receives, modifies, and transfers sensory information largely to specific regions of the cortex. In the two major MGB subdivisions, the ventral or lemniscal (MGV) and the dorsal or extralemniscal (MGD) divisions, cells often respond differently to acoustic stimuli (see Clarey et al. 1992 for a recent review). Extracellular recordings, made primarily in anesthetized cat but also from rodent and monkey, indicate that MGV thalamocortical neurons are arranged tonotopically, with many showing narrow frequency tuning and a consistent short-latency response to repeated sounds. MGD neurons, in contrast, are not tonotopically arranged and can display broad frequency tuning, more variable response latencies, and rapid habituation to repeated sounds (Aitkin and Webster 1971, 1972; Allon et al. 1981; Bordi and Ledoux 1994; Calford 1983; Calford and Webster 1981; Imig and Morel 1985). Currently it is not known how factors like membrane properties, dendritic architecture, or synaptic input features contribute to these distinct response differences. Moreover because some cells in one division may respond differently to auditory stimuli when compared with others in that same division (Aitkin and Webster 1971; Bordi and Ledoux 1994), it is not known whether these factors can be correlated with a particular response type.

Besides differing in response features, MGB neurons also differ morphologically. Cat and rat Golgi studies indicate that two main classes of thalamocortical neurons can be distinguished qualitatively in the two major subdivisions (Clerici and Coleman 1990; Clerici et al. 1990; Morest 1964, 1965a,b; Winer 1984). In MGV, ''tufted'' neurons have bushy secondary dendrites that result from lower-order dendrites giving rise to numerous branches in close proximity. In cat and rat, these cells are reported to have a restricted or ''bitufted'' domain polarized along the long axis of the cell body and parallel to the ascending fibers of the brachium of the inferior colliculus (IC). In the MGD, many neurons have ''stellate'' morphology due to radially extending, lower-order dendrites typically generating two higher-order dendrites that diverge to form a star-like configuration (Clerici and Coleman 1990; Clerici et al. 1990; Morest 1964, 1965b; Winer and Morest 1983, 1984). Some MGD neurons can have tufted-like morphology but do not display oriented dendritic trees (Clerici et al. 1990; Winer 1992).

Except for an early study (Nelson and Erulkar 1963), intracellular response features of MGB neurons in vivo are unavailable, but there are several reports of intracellular recordings in

slices. The surprising conclusion of the pioneer work of Jahnsen and Llinas (1984a,b) was that thalamocortical cells, including four from the MGB, displayed similar electrophysiological features regardless of morphological differences or thalamic location. This finding indicated that intrinsic membrane features were probably not related to cell to cell response differences to natural sensory stimuli in vivo. Recent work (Hu 1995; Hu et al. 1994; Senatorov et al. 1997) has challenged this perception in the auditory thalamus by proposing that rat MGV and MGD cells may have different intrinsic features that could influence their in vivo response. A hyperpolarization-activated cation current (I_h) found in most MGV neurons could produce a depolarizing ''sag'' that was not evident in most MGD neurons (Hu 1995). It was suggested that I_h produced more depolarized resting potentials in MGV neurons, putting them in the ''single spike,'' or tonic, mode. In contrast, MGD neurons without I_h were more hyperpolarized and in the Ca^{2+}-dependent ''burst mode'' of thalamic firing (Hu 1995; Hu et al. 1994; Jahnsen and Llinas 1984a). Given that a single thalamic neurons can switch between firing modes and that synaptic responses of cells in the two firing modes would differ when presented with the same input, control of resting potential is a potentially important feature in determining responses to sensory stimuli. However, the cells were selected populations from restricted regions of the MGV and MGD and only a few cells were labeled intracellularly (Hu 1995; Hu et al. 1994).

In addition to anatomic and extracellular response differences, the origin of afferent inputs to MGV and MGD cells differ as well. Most ascending MGV afferents arise from cells in the laminated, tonotopically organized central nucleus of the IC (Andersen et al. 1980; Calford and Aitkin 1983; Kudo and Niimi 1978, 1980; LeDoux et al. 1985; Rouiller and de Ribaupierre 1985). Ascending auditory inputs to MGD arise from other regions of the IC and the lateral tegmental system (see Winer 1992) and show no obvious laminar distribution. Recent evidence in the cat and rat (Peruzzi et al. 1997; St. Marie et al. 1997; Winer et al. 1996) indicates that some collicular inputs to both regions are GABAergic. The other major afferent inputs to MGB are excitatory inputs originating from auditory cortex and GABAergic inputs from the thalamic reticular nucleus (TRN) (Jones 1975; Jones and Powell 1969a,b; Jones and Rockel 1971; Montero 1983; Rouiller et al. 1985). TRN cells are organized topographically and project to both dorsal and ventral divisions (Crabtree 1998). Cortical inputs to MGB cells are mainly from layer VI pyramidal cells in primary auditory cortex (to MGV) or nonprimary auditory cortex (to MGD) the axons of which give rise to small, excitatory terminals thought to synapse on distal dendrites (Bajo et al. 1995; Ojima 1994; Rouiller and Welker 1991). Some evidence exists regarding the influence of these inputs on extracellular MGB cell responses in vivo (Ryugo and Weinberger 1976; Yan and Suga 1996; Zhang et al. 1997), but there are no data on their intracellular features.

In this study, we sought to clarify the relationship among cell location, cell morphology, intrinsic properties, and synaptic properties of MGV and MGD neurons. We recorded intracellularly from cells in both divisions of the rat MGB using brain slices and labeled these physiologically characterized cells. To correlate the membrane features and synaptic properties with morphology, the morphological type of a number of neurons was established using more quantitative methods. We then categorized and compared the basic membrane features of these different cell types in the two major divisions and compared the influences of ascending and descending synaptic inputs. Our analysis suggests that, in the rat slice, neurons in both regions with either cell morphology can have similar resting potentials, firing modes, proportion of response patterns to IC input (with one exception), and responses to corticothalamic and thalamic reticular nucleus stimulation. Overall our results imply that the marked contrast between the in vivo responses of MGV versus MGD neurons may be due to differences in the afferent response patterns and the selectivity of each afferent input to auditory stimuli.

METHODS

Intracellular recording

Methods for intracellular recording, stimulation, and labeling of MGB neurons are described elsewhere (Peruzzi et al. 1997; Smith 1992). All methods were approved by the University of Wisconsin Institutional Animal Care and Use Committee. Animals were maintained in an American Associations for Accreditation of Laboratory Animal Care-approved facility. Briefly, 3- to 6-wk-old hooded rats were anesthetized deeply (chloral hydrate, 70 mg/ml, 1–1.5 ml ip, or pentobarbital sodium, 10 mg/ml, 0.5 ml ip) and perfused transcardially with chilled, oxygenated sucrose saline (described in the following text). Four-hundred- to 500-μm slices in the desired plane of section containing the MGB were then made as described previously an placed in a holding chamber with oxygenated room temperature saline (Peruzzi et al. 1997; Smith 1992). After equilibrating, a slice was transferred to the recording chamber and perfused with oxygenated normal saline at 33–34°C containing the following (in mM): 124 NaCl, 5 KCl, 1.2 KH_2PO_4, 2.4 $CaCl_2$, 1.3 $MgSO_4$, 26 $NaHCO_3$, and 10 glucose. Sucrose saline contained sucrose instead of NaCl (Aghajanian and Rasmussen 1989). In experiments that assessed the effect of extracellular $[K^+]$ on membrane properties, we used a bathing solution which contained the following (in mM): 125 NaCl, 1.8 KCl, 1.2 KH_2PO_4, 1.8 $CaCl_2$, 1 $MgSO_4$, 26 $NaHCO_3$, and 10 glucose. This saline had a final $[K^+]$ similar to that used in previous in vitro MGB studies (Hu 1995; Hu et al. 1994).

In horizontal and sagittal slices, one stimulating electrode was positioned in the thalamic radiations (see Paxinos and Watson 1986, plates 84 and 103) to excite corticothalamic and thalamic reticular nucleus fibers. The other was placed in the brachium of the inferior colliculus to excite IC axons (see Peruzzi et al. 1997, Fig. 5).

Bicuculline methiodide, 2-hydroxysaclofen, DL-2-amino-5-phosphonovaleric acid (APV), 6,7-dinitroquinoxaline (DNQX), SR-95531 (Research Biochemicals International, Natick, MA), and CGP35348 (Ciba-Geigy, West Caldwell, NJ) were all mixed with artificial cerebrospinal fluid (ACSF) to the stated concentrations the day of the experiment and bath applied.

Glass microelectrodes (80–200 MΩ) filled with 2 M potassium acetate containing 2% Neurobiotin were used to record intracellularly. After recording and injection, the slice was removed from the recording chamber and fixed. Neurobiotin-labeled MGB neurons were prepared and reacted as previously described (Peruzzi et al. 1997; Smith 1992). Two-dimensional camera lucida drawings of injected cells were made at $\times$1,250. Cell body location relative to the MGB divisions was determined using the Paxinos and Watson (1986) atlas and the cytoarchitectural study of the rat MGB by Clerici and Coleman (1990).

Data analysis

PHYSIOLOGY. Intracellular current and voltage records were digitized and sampled by a PC using software developed here. The

difference between the voltage measured extracellularly in saline and intracellularly during recording was taken as the resting membrane potential. Input resistance was taken as the slope of the linear portion of the current-voltage plot near the resting potential or calculated from the maximum voltage deflection to a −0.1-nA current pulse. The *I-V* response was ''rectified'' if voltage responses to equal-amplitude, opposite-polarity currents differed by ≥25%. If the maximum voltage deflection to a 200-to 300-ms hyperpolarizing current differed from that during the last 25 ms by ≥2 mV, the cell was said to have a ''sag.'' Cells were in burst mode at rest if depolarization evoked a large long-lasting depolarizing event often crested by multiple high-frequency action potentials (see Fig. 3*B*). The burst depolarization depends on extracellular Ca^{2+} (not shown) and has been seen in MGB and elsewhere in the thalamus (Hu 1995; Jahnsen and Llinas 1984a,b; Tennigkeit et al. 1996).

Excitatory postsynaptic potential (EPSP) and short-latency inhibitory postsynaptic potential (IPSP) latencies were measured from stimulus artifact onset to where the PSP consistently changed the membrane potential. To dissociate EPSP and IPSP latencies when both were present, responses were recorded while the cell was polarized around rest. EPSP latencies were calculated near the IPSP reversal potential. $GABA_A$ IPSP latencies were measured as the time when an early component of the postsynaptic potential reversed polarity as membrane potential was changed from a depolarized to hyperpolarized level. Where applicable, first-spike latencies were calculated from the stimulus artifact onset to the action potential peak.

The number of EPSP amplitude levels was calculated by counting the number of levels that differed by >1 mV or that differed by >10% of the response amplitude, depending on which was greater, as stimulus intensity was increased from 10 to 150 V in 10-V increments.

Statistical analysis for all results was carried out using Minitab software (Minitab, State College, PA). Unless otherwise stated, statistical comparisons were performed using the Mann-Whitney test and the minimum criterion for statistical significance was $P < 0.05$.

ANATOMY. The somas and primary dendrites of labeled neurons were drawn at ×1,250, and soma areas were calculated using Neurolucida software (Microbrightfield, Colchester, VT). Only well-labeled somas with no signs of electrode induced deformation were used. Dendritic arbor area was measured using the same software by drawing a line between the ends of adjacent dendrites to create an area enclosing the entire dendritic tree, then measuring the enclosed area. Dendritic projection distance from the soma was calculated by measuring the length of the dendrite from the soma. Scaled circles representing 50 or 100 μm were used to count the number of dendrites extending beyond 50 or 100 μm, and the sum was termed the number of ''dendritic intersections'' at these radii. Each circle was centered around the soma center and divided into eight 45° sectors, and the number of dendrites intersecting each sector at 50 and 100 μm was counted. Also the number of sectors (directions) with one or more dendrites intersecting at 50 and 100 μm was counted. To estimate directional uniformity of dendritic projections, we devised a simple measurement termed the orientation ratio. This ratio is the sum of the number of dendritic intersections in the four sectors with the most intersections divided by the sum of the number in the four sectors with the fewest. If the sum of the four sectors with the fewest intersections totaled zero, it was set to one to avoid dividing by zero. A dendritic tree with similar numbers of dendrites projecting in each direction would have an orientation ratio close to one, whereas a tree with dendrites preferentially projecting in a small number of directions would have a large orientation ratio.

Analysis of the fully reconstructed dendritic trees of 23 neurons at ×1,250 demonstrated that stellate neurons had significantly longer dendrites than tufted neurons (Table 1, stellate range: 179–231 μm, tufted range: 123–176 μm). An additional 30 neurons were drawn at a lower magnification, and their dendritic lengths were measured. Those whose three longest dendrites averaged < 160 μm were called tufted and those that averaged > 175 μm were called stellate. A few of these neurons whose dendrites averaged between 160 and 175 μm could not be classified solely by dendritic length.

RESULTS

The database for this study consists of 106 MGB neurons that were recorded intracellularly. Certain aspects of some of the neurons have been considered in a previous study (Peruzzi et al. 1997).

Qualitative descriptions of MGV and MGD neurons

Figures 1 and 2 illustrate several examples of labeled thalamocortical cells from each MGB division. Cell somas had no consistent shape or size, regardless of MGB subdivision, plane of section, or dendritic tree appearance. The axon arose from the cell body or proximally from a primary dendrite (Figs. 1 and 2, ↑). No axon collaterals ever were observed within the MGB.

In the ventral division, dendritic trees were fairly dense and intertwined, resembling previous descriptions of dendritic tufts (Clerici et al. 1990; Winer 1992). MGV neurons sometimes displayed an oriented dendritic tree. For example, *cells 1, 2, 6,* and *7* in Fig. 1 demonstrate fairly clear orientation in the horizontal (*cells 1, 6,* and *7*) and sagittal (*cell 2*) planes. Other cells, including cells drawn in the coronal (*cells 5* and *8*) and horizontal planes (*cell 3*), did not display clear dendritic ori-

TABLE 1. *Morphological comparison of MGV and MGD neurons*

	MGV 7H, 2S, 1C 10	MGD 12H, 1C 13	Tufted <40,000 12	Stellate >40,000 6
Dendritic tree area, μm^2	28,600 ± 5,900	45,700 ± 20,300	29,300 ± 5,800[a]	62,800 ± 12,700
Soma area, μm^2	190.2 ± 45.0 (19)	181.6 ± 46.2 (23)	175.7 ± 33.0 (8)	182.2 ± 44.5 (4)
Dendrite length, μm	133.0 ± 8.6[b] (9)	181.5 ± 31.1 (11)	140.4 ± 14.4[c]	204.7 ± 19.2
Number of intersections >50 μm	42.0 ± 8.8[d]	31.5 ± 6.7	38.9 ± 9.2[c]	29.7 ± 5.9
Number of intersections >100 μm	19.7 ± 10.6	25.1 ± 9.4	20.0 ± 8.4[c]	32.8 ± 5.4
Number of directions >50 μm	7.6 ± .7	7.4 ± .7	7.4 ± .7	7.7 ± .5
Number of directions >100 μm	5.5 ± 1.6	6.5 ± 1.7	5.8 ± 1.6[e]	7.7 ± .5
Orientation ratio at 100 μm	7.8 ± 5.2	6.1 ± 3.8	8.3 ± 4.7[a]	3.4 ± .6

Number of neurons drawn in the horizontal, sagittal, and coronal planes for the dorsal and ventral medial geniculate body (MGD and MGV) are 12, 0, and 1 and 7, 2, and 1, respectively. Neurons were grouped based on dendritic tree area into small area neurons (<40,000 μm^2) and large area neurons (>40,000 μm^2), which corresponds to tufted and stellate morphologies, respectively. Description of each measurement is found in the text. Values are means ±SD, with *n* in parentheses. [a] Significantly different than stellate, $P < 001$. [b] Significantly different than MGD, $P < 0.005$. [c] Significantly different than stellate, $P < 0.05$. [d] Significantly different than stellate, $P < 0.005$. [e] Significantly different than MGD, $P < 0.001$.

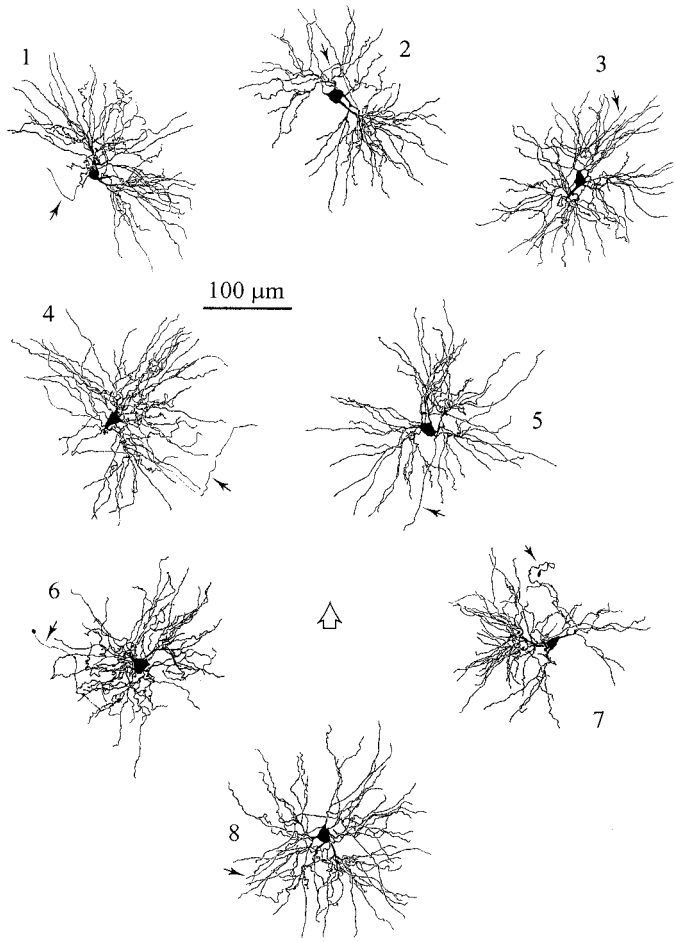

FIG. 1. Camera lucida drawings of Neurobiotin-labeled ventral medial geniculate body (MGV) neurons. Quantitative analysis of MGV dendrites indicates that all our labeled MGV neurons have tufted morphology, characterized by shorter dendrites that branch profusely within 50 μm of the cell body, with varying degrees of dendritic tree orientation. *Neurons 1, 3, 4, 6,* and *7* were drawn in the horizontal plane, with rostral toward the *page top* (⇑) and lateromedial represented horizontally on the page. *Neurons 5* and *8* were drawn in the coronal plane, with dorsal toward the *page top* and lateromedial represented horizontally. *Neuron 2* was drawn in the sagittal plane, with dorsal toward the *page top* and rostrocaudal represented horizontally on the page. Some MGV tufted neurons have dendrites that preferentially project in certain directions (*neurons 1, 2, 4, 6,* and *7*), while other neurons in both the horizontal and coronal planes have dendrites that project in all directions in the plane (*neurons 3, 5,* and *8*). ↓, axons. Scale bar applies to all cells.

entation but rather projected in all directions in the plane. The primary dendrites of MGV neurons were fairly smooth, whereas higher-order dendrites had irregular surfaces with noticeable protrusions but very few dendritic spines.

Some MGD neurons had tufted dendritic trees resembling those in the ventral division, with a comparable number of primary dendrites that branched profusely and showed varying amounts of orientation (Fig. 2, *cells 2–5*). Another group had larger dendritic trees that did not branch as profusely and extended in all directions in the horizontal or coronal planes, conforming to earlier descriptions of MGD cells with ''stellate'' morphology (Clerici et al. 1990; Winer 1992) (Fig. 2, *cells 1,* and *6–8*). However, it was often difficult to qualitatively assess whether the features of these neurons, for example dendritic length, branchiness of the dendritic trees close to the cell body, and dendritic orientation, could distinguish stellate versus tufted morphology. Therefore we made a series of measurements on the dendritic arbors of several well-filled MGB neurons to see more objectively whether two distinct dendritic morphologies are indeed found in MGB.

Quantitative analysis of somas and dendrites of MGB thalamocortical neurons

Measurements were made on 42 cell bodies, 19 from MGV and 23 from MGD. Table 1 shows that the measured soma areas were similar in dorsal and ventral divisions. Also compared in Table 1 are the dendritic characteristics of 10 well-labeled MGV neurons and 13 well-labeled MGD neurons. Ventral division neurons had a fairly small range of arbor areas (20,000–35,000 μm^2). MGD neurons, by contrast, had two separate area ranges, with a total range of 19,000–81,000 μm^2. One range of MGD areas overlapped with the MGV areas, whereas the other range was significantly larger and did not. Therefore we classified neurons with dendritic areas <40,000

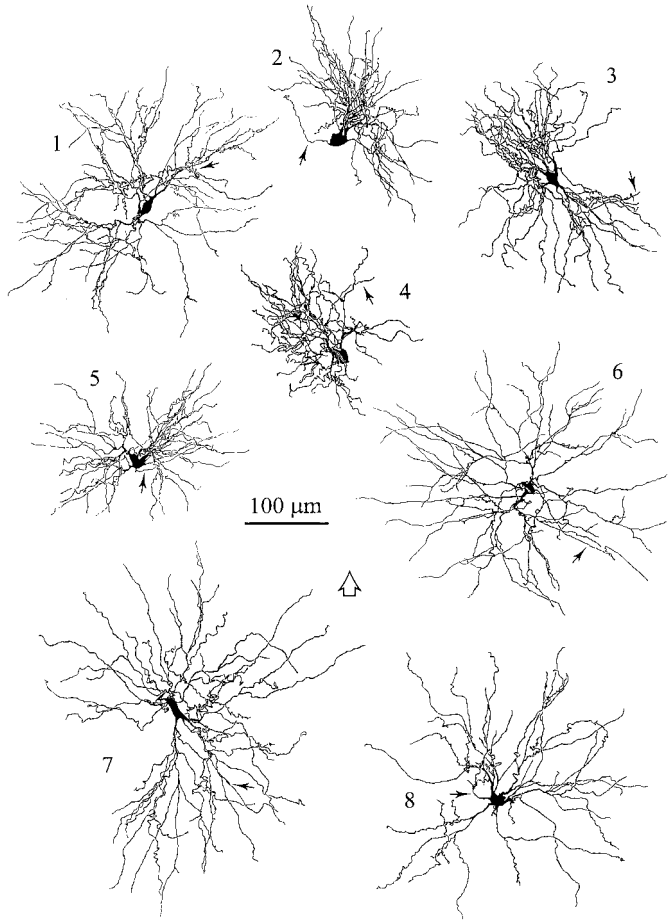

FIG. 2. Camera lucida drawings of Neurobiotin-labeled dorsal medial geniculate body (MGD) neurons. Examples of the 2 distinct morphologies in MGD revealed by quantitative analysis of MGD dendrites. *Neurons 1, 6, 7,* and *8* have stellate morphology, characterized by long dendrites that branch moderately in all directions and have distal dendritic branchpoints. *Neurons 2–5* have tufted dendritic morphology that is similar to the morphology of MGV neurons. Some tufted neurons (especially *neurons 2–4*) have dendritic arbors that project preferentially in certain directions, with sparser projections in other directions. *Neurons 2–8* were drawn in the horizontal plane. *Neuron 1* was drawn in the coronal plane. Orientation of the neurons on the page is the same as in Fig. 1. ↓, axons. Scale bar applies to all cells.

μm^2 as small area neurons and neurons with dendritic areas $>40{,}000$ μm^2 as large area neurons and then analyzed the dendritic characteristics of the two groups. The dendritic areas of the small area MGD neurons were 27,800 μm^2 on average, comparable with the average MGV area (Table 1), whereas those of the large area MGD neurons were 62,800 μm^2. Measuring the three longest dendrites revealed that small area neurons in both divisions had similar dendrite lengths. Dendrites of MGD large area neurons were significantly longer (see Table 1), indicating that differences in dendritic tree area was at least partially due to a difference in dendrite length.

Grouping cells according to the area of their dendritic trees revealed other consistent differences between the two populations. The number of dendritic intersections (see METHODS) for small area neurons in either MGV or MGD was significantly larger than for large area neurons at 50 μm, but significantly smaller at 100 μm. This result indicates that small area arbors were more exuberant at 50 μm and that many small area neuron dendrites ended between 50 and 100 μm from the soma. When the number of sectors intersected (see METHODS) was measured, at 50 μm, small and large area dendrites extended almost omnidirectionally, with most neurons having dendrites intersecting seven or eight of eight possible sectors. Dendrites of large area neurons continued to project in all directions 100 μm from the soma, but dendrites of small area neurons on average projected through only six of eight possible sectors. Shorter dendrites and more ''oriented'' (see following text) dendritic tree characteristics of small area neurons probably contributed to the decrease in the number of sectors intersected at 100 μm. Orientation ratios (see METHODS) for large area neurons at 100 μm were significantly smaller (Table 1), i.e., large area neuron dendrites are less oriented. However, it should be noted that 6/17 small area neurons had ratios similar to large area neurons at 100 μm, supporting our qualitative observation that not all small area cells have strongly oriented dendritic arbors. Finally, we found that small area cell dendrites in both MGV and MGD tended to have all branching occur 20–60 μm from the soma, whereas large area dendritic branching occurred fairly evenly 20–120 μm from the soma. Examples of distal branchpoints are seen in all the large area arbors in Fig. 2 (*cells 1,* and *6–8*). Based on these quantitative results, the small area neurons conform to qualitative descriptions of tufted neurons, whereas the dendritic characteristics of the large area neurons conform to descriptions of stellate neurons. Although the distribution of dendritic lengths of tufted (small area) and stellate (large area) neurons was nonoverlapping, individual tufted neurons could have nonoriented dendritic arbors, and individual stellate dendrites could have branching nearly as dense as typical tufted arbors.

Intrinsic properties of MGB neurons

The intrinsic properties of 31 MGV neurons and 25 MGD neurons were analyzed in detail. As shown in Table 2, the average resting membrane potential and average input resistance were similar throughout the MGB regardless of location or cell type. Suprathreshold depolarizing current pulses elicited burst firing in about one-third of the MGV and MGD neurons, characterized by a large hump crested by one or more action potentials in a high-frequency burst (Fig. 3*B*). This response was not confined to a particular cell type. Cells in the burst firing mode had a resting potential of -69.8 ± 3.3 (SD) mV. All MGB neurons could generate the burst after the offset of hyperpolarizing current (a rebound burst, Fig. 3, *A* and *B*). The average number and frequency of action potentials in the rebound burst was similar throughout the MGB (Table 2). The resting potential of bursting neurons was significantly more hyperpolarized than those showing the tonic, or sustained, firing mode at rest. The tonic firing mode, which is similar to the ''single-spike'' mode of previous studies (Hu 1995; Hu et al. 1994), was characterized by firing for all or most of the duration of the current injection (Fig. 3*D*). Neurons in this firing mode had an average resting potential of -61.7 ± 4.4 mV and could be either morphology. Firing rate increased and first-spike latency decreased with increasing current (Fig. 3*D*). About half of the neurons in the tonic firing mode displayed noticeable spike rate adaptation. Switching the membrane potential by injecting constant current into a cell changed the firing mode of the neuron, indicating that the ability to burst or fire tonically is possessed by all MGB neurons.

TABLE 2. *Comparison of intrinsic properties versus MGB subdivision*

	MGD	MGV
n	25	31
V_{rest}, mV	-64.7 ± 6.4	-64.3 ± 4.9
R_{in}, MΩ	68 ± 29	61 ± 31
Percent burst at rest	36 (9)	32 (10)
Percent with sag	20 (5)[a]	61 (18)
Freq. Ca^{2+} burst (Hz)	338 ± 51	365 ± 86
Number of spikes in rebound	3.4 ± 1.6	3.4 ± 1.2
After hyperpolarization maximum amplitude, mV	2.8 ± 1.9	2.5 ± 1.6
Rectification	15/25	18/26

n is the number of neurons. For percentage of neurons that burst and percentage of neurons with sag, the number in parentheses indicates the actual number of neurons observed with a burst or sag. All values shown are means $\pm$ SD. [a] Significantly different than MGV, $P < 0.005$, χ^2 test.

In our normal saline, there was no segregation of cells, based on anatomic type or location, into a particular firing mode. Because the finding that MGV and MGD neurons have similar resting potentials differs from previous reports comparing MGV and MGD neurons (Hu 1995; Hu et al. 1994), extracellular $[K^+]$ was changed to match values used in the previous studies. Cells switched from our normal saline to one containing 3 mM $[K^+]$ showed a consistent hyperpolarization of the membrane potential (3–5 mV) in both dorsal and ventral divisions. This manipulation could change a nonbursting cell into the burst firing mode or lower the amount of current needed to generate a burst in an already bursting cell. However, the lower extracellular $[K^+]$ did not divide MGB neurons into tonic-firing MGV and burst-firing MGD populations. Also, because the preparation used in previous studies restricted the region of MGB that could be sampled, neurons in the rostral quarter and the medial third of the MGV and MGD were excluded. When the remaining neurons were analyzed, the average resting membrane potential and proportion of neurons bursting at rest were similar between MGV and MGD. Finally, 15 MGD stellate and 12 MGV tufted neurons were identified anatomically (see METHODS), and their intrinsic properties were compared. Again, all measured properties were similar with one exception. This exception was the prevalence of a depolarizing

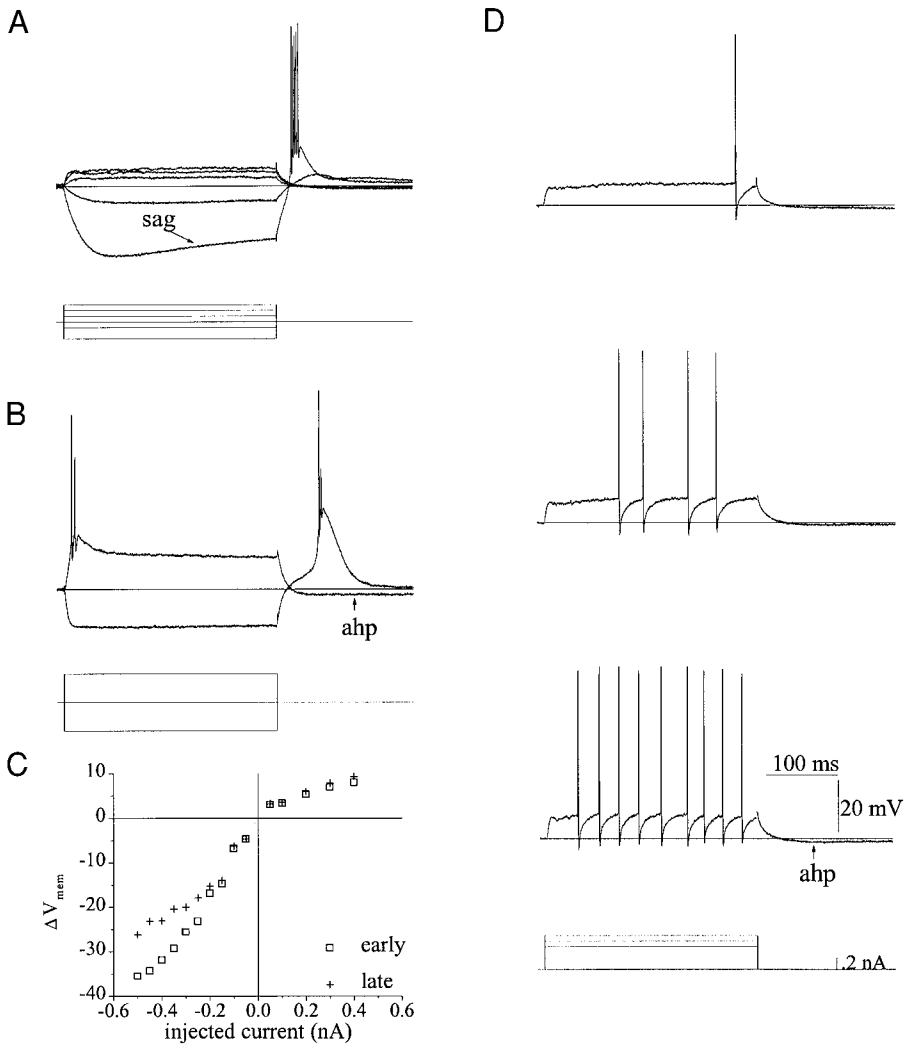

FIG. 3. Intrinsic properties of medial geniculate body (MGB) neurons. *A*: responses of a MGV tufted neuron (*top*) elicited by polarizing current pulses (*bottom*). Larger (−0.3 nA) hyperpolarizing current pulse generated a depolarizing sag (→) and a rebound burst. Equal but opposite current pulses caused a smaller voltage change in the depolarizing direction indicating rectification. V_{rest} = −63 mV. *B*: responses of a MGD tufted neuron (*top*) to +0.5- and −0.5-nA pulses (*bottom*). Cell responded to the depolarization with a burst from resting potential followed by a long-lasting afterhyperpolarization (ahp, ↑) that persisted for hundreds of milliseconds. This cell also exhibited no sag and a rebound burst. V_{rest} = −69 mV. *C*: *I-V* curve for the neuron in *A* and *D* illustrating the rectification in the depolarizing direction and the sag in the hyperpolarizing direction. Voltage changes were averaged for time windows 10–30 ms (early) and 270–290 ms (late) after the start of current injection. *D*: same neuron as in *A*. Suprathreshold responses (*top 3 traces*) to 0.4- to 0.6-nA current pulses (*bottom*). Latency to firing decreased and firing frequency increased as the amount of current increases. In some neurons, large current injections evoked an initial spike at the onset of the current (not shown). ahp (↑) can be seen after the 0.6-nA current injection. Scale bars in *D* apply to *A*, *B*, and *D*.

''sag'' during a hyperpolarizing current pulse in most MGV neurons (Fig. 3*A*), which occurred only in a small number of MGD neurons (Table 2). Of the four identified MGD cells showing the sag, two (small sags in these neurons) had stellate morphology, and two had tufted morphology. The *I-V* curve in Fig. 3*C*, comparing the peak change in membrane potential (□) with the change observed just before current offset (+) in an MGV neuron, reflects this sag as well as an outward rectification. The sag is thought to reflect activation of a Cs^+-sensitive, mixed cation current (I_h) (Hu 1995; Tennigkeit et al. 1996). Also, a smaller voltage deflection was observed for depolarizing compared with hyperpolarizing currents in most MGB neurons (Fig. 3, *A* and *C*). The rectification probably reflected 4-aminopyridine-sensitive K^+ currents activated by membrane depolarization in MGB and lateral geniculate nucleus neurons (McCormick 1991; Tennigkeit et al. 1996, 1998). Another possible effect of K^+ current activation is the afterhyperpolarization (ahp) that often occurred after the offset of depolarizing current and could last hundreds of milliseconds (Table 2, Fig. 3*B*).

IC inputs to MGB neurons

We previously described direct excitatory and inhibitory IC inputs to MGB neurons (Peruzzi et al. 1997). Over half of the tufted and stellate cells reported in this study (38/72) received both, but there were variations. Figure 4 illustrates the four patterns of IC synaptic input seen when colliculogeniculate axons were stimulated electrically in the brachium of the inferior colliculus (BIC). These patterns were named based on the presence of a $GABA_A$ IPSP and its latency relative to the EPSP latency. MGB neurons with only excitatory IC input were called EX/O. EX is for ''excitatory'' and O signifies a lack of an apparent $GABA_A$ IPSP (Fig. 4, *E* and *F*). Neurons with only inhibitory IC input were named IN/O, IN is for ''inhibitory'' IPSP and O signifies a lack of a driven EPSP (Fig. 4, *G* and *H*). If a $GABA_A$ IPSP preceded the EPSP, the response was called IN/EX (Fig. 4, *A* and *B*), and if the EPSP preceded the IPSP, it was called EX/IN (Fig. 4, *C* and *D*). Because neurons with $GABA_A$ IPSPs almost always had a $GABA_B$ component (43/44 of the IC inputs, 68/73 of the descending inputs described in the following text), the $GABA_B$ component was not included in the nomenclature. With one exception (see following text), both tufted and stellate could show any of the four patterns of synaptic inputs, and in this small sample of cells, there was no obvious difference in the distribution of the four patterns between the two cell types in the two MGB divisions studied.

When gradually increasing the shock strength applied to the

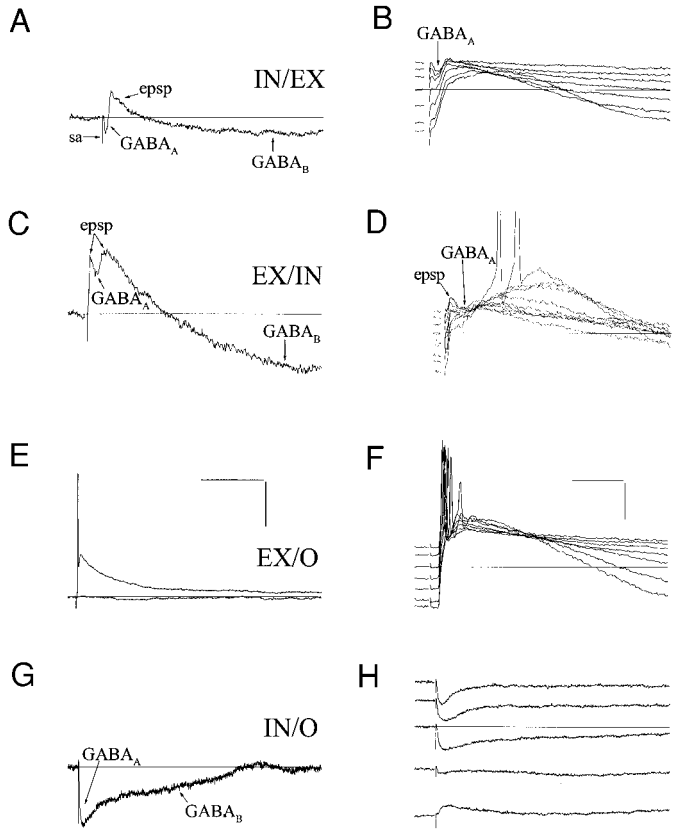

FIG. 4. Patterns of inferior colliculus (IC) synaptic responses. Responses for 4 cells at a single membrane potential (*left*) and when polarized around rest (*right*, horizontal line represents resting membrane potential). *A* and *B*: representative $GABA_A$ inhibitory/excitatory postsynaptic potential (IN/EX) response in a MGV neuron. Electrical stimulation of the brachium of the inferior colliculus (BIC) produces a stimulus artifact (sa) followed by $GABA_A$ inhibitory postsynaptic potential (IPSP), excitatory PSP (EPSP), and $GABA_B$ IPSP, in that order. $V_{rest} = -61$ mV. $V_{mem} = -55$ mV in *A*. For this figure and all following figures, the sa has been truncated. *C* and *D*: representative excitatory/inhibitory PSP (EX/IN) response in a MGV tufted neuron. BIC stimulation produced an EPSP, a $GABA_A$ IPSP, and a $GABA_B$ IPSP, in that order. Trace in *C* is at V_{rest} (-68 mV). *E* and *F*: representative all-or-none excitatory only (EX/O) response in a MGV neuron. Trace in *E* has a longer duration to illustrate response duration. In *E*, no response was recorded at 1 stimulus intensity (*flat trace*) but a slight increase in stimulus intensity generated a suprathreshold response with a long-lasting EPSP. Many, but not all EX/O responses were all or none (see Fig. 5*A*). Trace in *E* is at V_{rest} (-64 mV). *G* and *H*: representative inhibitory only (IN/O) response in a MGV tufted neuron. Trace in *G* has a longer duration to illustrate the $GABA_B$ time course and is at V_{rest} (-64 mV). Scale bars in *E* apply to *A, C, E,* and *G*. For this and all subsequent figures, *x* is the horizontal scale bar and *y* is the vertical scale bar. *A* and *C*: $x = 25$ ms, $y = 5$ mV; *E*: $x = 100$ ms, $y = 20$ mV; *G*: $x = 100$ ms, $y = 5$ mV. Scale bars in *F* apply to *B, D, F,* and *H*. *B* and *D*: $x = 10$ ms, $y = 10$ mV; *F*: $x = 10$ ms, $y = 20$ mV; *G*: $x = 40$ ms, $y = 10$ mV.

BIC, the EPSPs and IPSPs often had multiple discernible amplitudes, implying that multiple IC fibers converge onto single MGB neurons. The number of excitatory inputs converging on a single MGB neuron was small, with two to four distinguishable amplitudes in most cases (3.0 ± 1.9) (Fig. 5, *A* and *B*). Multiple levels of excitation were noted for all response patterns. In most cases, the multiple peak amplitudes were not due to the addition of an increasing inhibition to a constant excitation because peak amplitude increased with stimulus intensity. Also, multiple peak amplitudes still were noted when the $GABA_A$ channel was blocked (not shown). Inhibitory IC inputs occasionally were isolated either by application of glutamate channel blockers APV and DNQX or by stimulation of only inhibitory fibers. Similar to the excitatory fibers, increasing the shock stimulus amplitude generated multiple IPSP amplitude levels (Fig. 5, *C* and *D*). In most cases, the $GABA_B$ IPSP had the same, or a slightly higher, stimulation threshold as the $GABA_A$ IPSP (Fig. 5, *C* and *D*). Thus more than one IC inhibitory input also converges onto MGB relay neurons. Generally, the number of discernible excitatory levels was independent of input class, but some of the EX/O neurons received a large, all-or-none EPSP. An example is shown in Fig. 4*E*. When the intensity of the stimulus was low, no response above baseline was seen. Increasing stimulus intensity slightly evoked a large suprathreshold EPSP. Although it is difficult to tell if subsequent smaller EPSPs were obscured, the evoked response size and duration did not change as stimulus intensity was increased further, suggesting that only one fiber was being stimulated.

Neurons receiving each type of IC input were found in similar proportions in the dorsal and ventral divisions. Table 3 shows that there are approximately equal numbers of neurons receiving EX/O and IN/EX input, the two most common classes of input. However, only neurons with tufted morphology received a single, large, suprathreshold EPSP. There was a higher percentage of EX/IN neurons in the dorsal division (23%) than in the ventral division (7%), but the difference was not statistically significant. About 10% of the neurons in either subdivision received exclusively inhibitory IC input. It is possible that some cells exhibiting EX/O or IN/O patterns actually receive both excitatory and inhibitory inputs from the IC because a small number of EX/O responses also showed a long-duration IPSP (probably $GABA_B$ mediated), but the stimulus electrodes only excited the fiber type whose response was observed.

The PSP latency was related to the type of IC input. For these monosynaptic inputs to MGB neurons, PSP latency provides a measure of the relative axonal conduction velocity of each input. The EPSP latencies of EX/O inputs were significantly shorter than the latencies of IN/EX EPSPs (Table 3) in both subdivisions. Bath application of the $GABA_A$ antagonists bicuculline or SR95531 to neurons with IN/EX or EX/IN IC inputs did not change the EPSP latency (Fig. 6,*C* and *E*). Early $GABA_A$ IN/EX IPSPs had similar latencies to the EX/O cell EPSPs throughout the MGB (Table 3), suggesting that axons giving rise to EX/O excitatory input and IN/EX inhibitory input had similar, relatively fast conduction velocities. MGV neurons with EX/IN inputs had $GABA_A$ IPSP latencies like IN/EX $GABA_A$ latencies, but their EPSP latencies were among the fastest observed. In contrast, MGD $GABA_A$ IPSPs in EX/IN cells were significantly longer than all other $GABA_A$ latencies, whereas the EPSP latencies for these neurons were significantly shorter than the IN/EX EPSP latencies. IN/O $GABA_A$ latencies were comparable with the $GABA_A$ latencies of IN/EX inputs. On the basis of these results, IC excitatory input can be subdivided into short-latency inputs, which are generally seen in EX/O or EX/IN categories, and long-latency inputs, which are generally in the IN/EX category. The inhibitory IC inputs also can be grouped according to latency. Shorter-latency IPSPs are associated with IN/EX, IN/O, and MGV EX/IN inputs, whereas longer-latency IPSPs occur in MGD EX/IN responses.

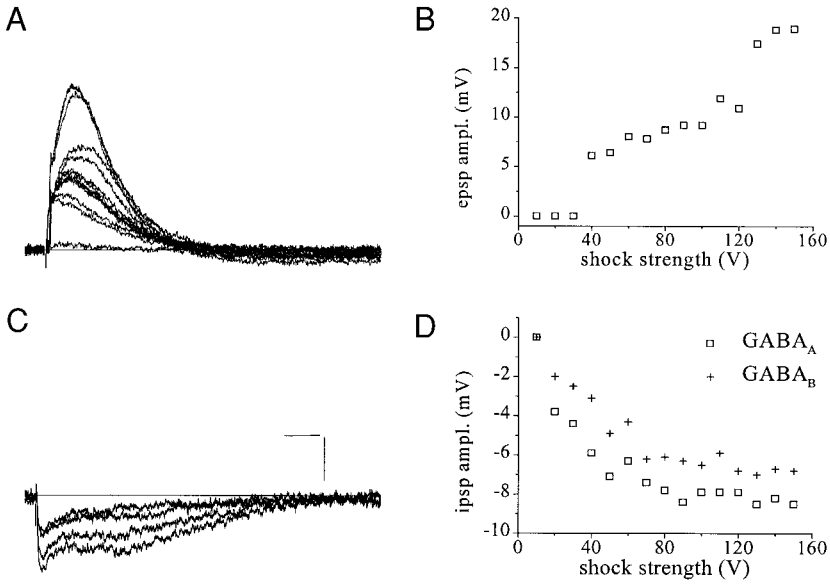

FIG. 5. Multiple IC excitatory and inhibitory inputs can converge on a single MGB neuron. *A*: synaptic responses of a MGD stellate neuron to BIC stimulation as stimulus intensity was increased from 10 to 150 V in 10-V steps. Increasing intensity generated 4–5 distinguishable EPSP amplitudes. For clarity, not all traces are shown. $V_{rest} = -68$ mV. *B*: peak EPSP amplitude vs. shock intensity of BIC stimulation for the neuron in *A*. *C*: records from a different MGD neuron showing multiple IPSP amplitudes for $GABA_A$ and $GABA_B$ IPSPs to increasing shock strength while excitation was blocked by DL-2-amino-5-phosphonovaleric acid (APV) and 6,7-dinitroquinoxaline (DNQX). Again, not all traces are shown. $V_{mem} = -54$ mV. *D*: IPSP amplitude vs. shock strength for the same neuron as in *C*, for the early and late IPSP components. Scale bars, *A*: $x = 20$ ms, $y = 5$ mV; *C*: $x = 50$ ms, $y = 5$ mV.

Pharmacology of IC inputs

EPSPs for stellate and tufted neurons had both α-amino-3-hydroxy-5-methyl-4-isoxazolepropionic acid (AMPA) and *N*-methyl-D-aspartate (NMDA) components. There was considerable variation in how much each component contributed to the EPSP. Like other dual component glutamatergic EPSPs, blocking AMPA channels diminished the fast portion of the EPSP, resulting in a reduced peak amplitude and a longer time to peak. Figure 6*A* shows a MGV tufted neuron response that still has a large NMDA component during application of the AMPA channel antagonist DNQX. Blocking the AMPA-mediated EPSP prevented a spike from occurring, even when a sizeable NMDA-mediated EPSP remained (Fig. 6*A*, same cell as in Fig. 4, *E* and *F*). Figure 6*B* shows a MGD stellate neuron where DNQX largely abolished the EPSP. Conversely, in a different neuron, blocking NMDA receptors with APV slightly reduced the EPSP amplitude but significantly reduced the EPSP's area and duration (Fig. 6*D*, *middle* vs. *bottom*). The effect of APV persisted even at hyperpolarized membrane potentials for suprathreshold and subthreshold IC inputs. From the same neuron as in Fig. 6*D*, Fig. 6*E* demonstrates that blocking the NMDA component effectively prevented the Ca^{2+} burst at -86 mV. An IC-evoked NMDA component at hyperpolarized membrane potentials was seen in three other cells tested in APV.

We also tested the effect of the monosynaptic $GABA_A$ IPSP (Peruzzi et al. 1997) on the IC-evoked EPSP. Bath application of the $GABA_A$ receptor antagonists bicuculline or SR95531 resulted in a larger, longer lasting EPSP in cells with IN/EX IC inputs (Fig. 6, *D* and *E*, *middle*, and *C*, 5/5 cells tested) and with EX/IN IC inputs (not shown, 2/2 cells tested), but they had little effect on cells with EX/O IC inputs (2/3 cells tested). In two MGD neurons, blocking $GABA_A$ receptors uncovered a suprathreshold EPSP (Fig. 6, *D* and *E*). In the MGV, however, the EPSPs revealed by drug application were subthreshold at rest (Fig. 6*C*, $n = 5$).

Timing of BIC evoked first-spike latencies

Typically, because of the Ca^{2+} burst and other voltage-dependent conductances, synaptically generated first-spike la-

TABLE 3. *Patterns and latencies of synaptic input to MGB neurons*

	IC Inputs				Descending Inputs			
	IN/EX	EX/IN	EX/O	IN/O	IN/EX	EX/IN	EX/O	IN/O
n								
MGV	16/41	3/41	17/41	5/41	46/60	1/60	11/60	2/60
MGD	12/31	7/31	9/31	3/31	21/31	0/31	7/31	3/31
EPSP latency, ms								
MGV	3.8 ± 1.3[a]	1.1 ± .3[b]	2.3 ± 1.3	na	3.4 ± 1.0	2.3	3.2 ± 1.1	na
MGD	4.1 ± 1.8[a]	2.6 ± .7[b]	2.2 ± 1.0	na	3.7 ± 1.2	na	2.9 ± 1.5	na
$GABA_A$ latency, ms								
MGV	2.0 ± .6[c]	2.0 ± .1[c]	na	1.7 ± .6	1.8 ± .5	1.6	na	1.7 ± .7
MGD	2.1 ± .5[c]	4.7 ± .8[d]	na	2.0 ± 1.2	1.9 ± .6	na	na	2.1 ± .8
$GABA_B$ present								
MGV	16/16	3/3	2/17	5/5	41/46	1/1	2/11	2/2
MGD	12/12	7/7	4/9	2/3	20/21	0/0	3/7	3/3

n is the number of each pattern of synaptic input in each subdivision. Values are means ±SD. IN/EX and EX/IN, $GABA_A$ inhibitory postsynaptic potentials (IPSPs) preceded excitatory PSPs (EPSPs) and vice versa, respectively; EX/O and IN/O, only excitatory and only inhibitory, respectively, inferior colliculus input. [a] Significantly different than EX/O EPSP latency, $P < 0.001$. [b] Significantly different than IN/EX EPSP latencies, $P < 0.05$. [c] Not significantly different than EX/O EPSP latency, $P > 0.05$. [d] Significantly different than IN/EX and IN/O IPSP latencies, $P < 0.001$.

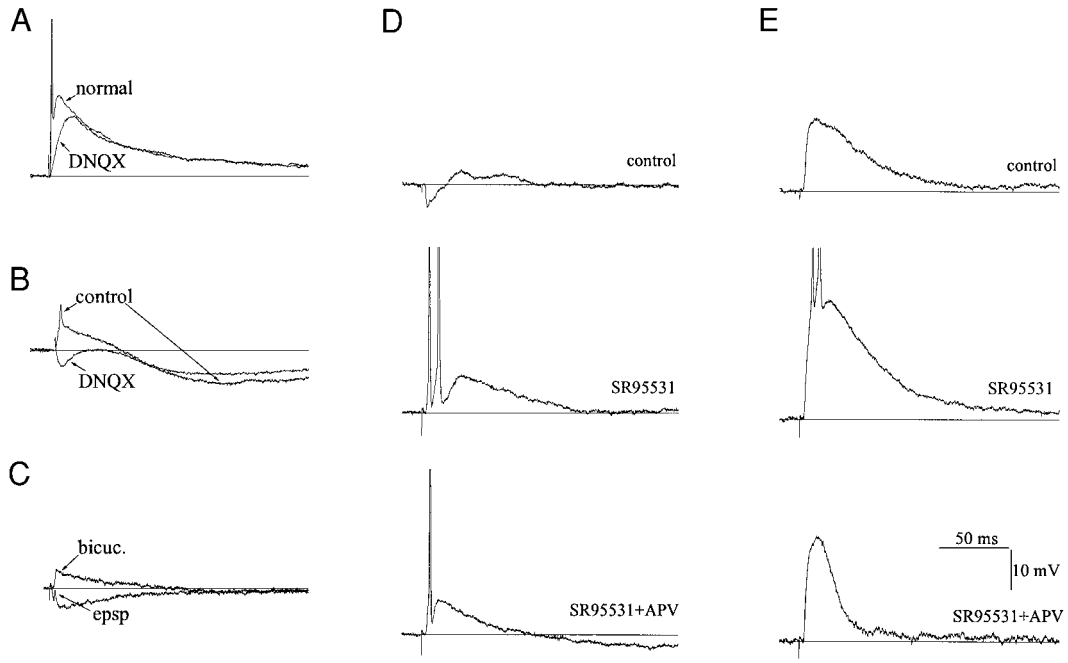

FIG. 6. Effect of drugs on MGB responses to BIC stimulation. *A*: responses of an EX/O MGV neuron to suprathreshold stimulation of the BIC in normal saline and in saline containing the α-amino-3-hydroxy-5-methyl-4-isoxazolepropionic acid (AMPA)/kainate glutamate receptor antagonist DNQX. *B*: responses of an EX/IN MGD stellate neuron to BIC stimulation in normal saline and saline containing DNQX. In DNQX the EPSP is abolished while the IPSPs are left intact. $V_{mem} = -58$ mV. *C*: responses of an IN/EX MGV tufted neuron in normal saline and in saline containing the $GABA_A$ receptor antagonist bicuculline (bicuc.). In bicuculline, the early IPSP was abolished more fully exposing the EPSP. $V_{mem} = -58$ mV. *D*: response of an IN/EX MGD cell to BIC shock stimulation of the same strength in normal saline, in saline containing the $GABA_A$ receptor antagonist SR95531 or in saline containing SR95531 and APV at a depolarized $V_{mem} = -52$ mV. SR95531 blocked the early IPSP and exposed a large suprathreshold response (*middle*). A significant NMDA component of the EPSP was found by stimulation during application of the *N*-methyl-D-aspartate (NMDA) receptor antagonist APV (*bottom*). Removal of the late NMDA component of the EPSP reduced the spike output and uncovered a $GABA_B$ IPSP. *E*: response of the same neuron in the same solutions at a $V_{mem} = -86$ mV. NMDA component appears to be necessary for the neuron to burst at hyperpolarized V_{mem} (*middle* and *bottom*). Action potentials in *A, D,* and *E* were truncated. Scale bars in *E* apply to *A–E.*

tencies of thalamic neuron are highly dependent on membrane potential (Fig. 7, *A–C*) (Hu et al. 1994; Jahnsen and Llinas 1984a,b; McCormick 1991). However, two neurons with IN/EX IC input exhibited exceptionally consistent first-spike latencies that were independent of the membrane potential (Fig. 7, *D–F*). Figure 7*A* illustrates a MGD tufted cell with an EX/O IC input. Cells with this input were typically suprathreshold at both depolarized and hyperpolarized membrane potentials. The first-spike latency (FSL) was fairly consistent at membrane potentials depolarized above levels where the Ca^{2+} burst would be strongly activated (Fig. 7*C*, points above -70 mV). When hyperpolarized into the calcium burst mode of firing, cells increased their FSL as hyperpolarization increased (Fig. 7*C*, points below -70 mV). Changes in FSL >10 ms were observed in some cases. The increased FSL appeared to be caused by slow activation of the Ca^{2+} burst (Fig. 7*B*). In contrast to the EX/O cells, IN/EX and EX/IN cells usually generated synaptically induced spikes only at membrane potentials positive to -60 mV. Figure 7, *D–F*, illustrates one of the two neurons with IN/EX IC input that was suprathreshold at rest and its unusual spike response. Over a 40 mV range, the FSL change was only 400 μs. Even when in the Ca^{2+} burst firing mode (Fig. 7*E*), the action potential was evoked at a fixed latency. Only the first spikes were well timed, later spikes were not (Fig. 7*D*, later spikes).

Although we did not investigate the effects of bicuculline on the neurons with well-timed FSLs, we did look at FSLs of one neuron with IN/EX IC input and one with EX/IN IC input during blockade of $GABA_A$. In these two neurons, one of which is shown in Fig. 6, *D* and *E*, *middle*, the timing of FSL was similar to that of the EX/O neurons. This result supports the idea that the inhibition is necessary to produce the consistent first spike latency.

Descending inputs to MGB neurons: corticothalamic EPSPs and TRN IPSPs

In horizontal or sagittal slices, we also could stimulate the descending corticothalamic (CT) and thalamic reticular nucleus (TRN) inputs in the thalamic radiations. Activating these descending axons elicited a much more standardized response than IC stimulation, eliciting a $GABA_A$ IPSP/EPSP/$GABA_B$ IPSP sequence in 74% of both tufted and stellate neurons throughout the MGB (Fig. 8, *A* and *B*, and Table 3). The remainder received only excitatory corticothalamic input (EX/O, 20%) or only inhibitory TRN input (IN/O, 5%). Again, we cannot be certain whether EX/O and IN/O patterns reflect the true innervation or the selective stimulation of one fiber type.

Postsynaptic potential latencies were fairly uniform, regardless of neuron location or anatomic type (Table 3). Unlike IC inputs, there was no significant difference in the corticotha-

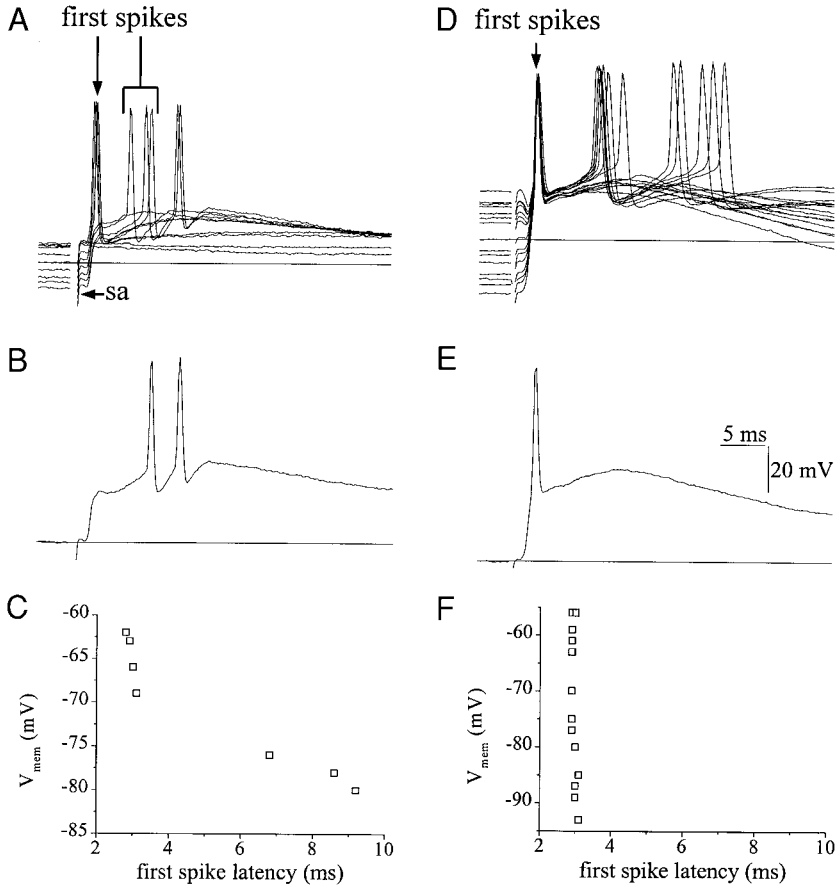

FIG. 7. First-spike latency (FSL) of MGB responses to BIC stimulation. *A*: suprathreshold responses of an EX/O tufted neuron in the MGD to the same BIC stimulation at various membrane potentials. FSL of action potentials are fairly consistent for membrane potentials more than −70 mV (↓) but increase substantially for V_{mem} less than −70 mV (spikes in brackets). *B*: example of a burst response in the same neuron at V_{mem} equal to −80 mV, with an initial fast EPSP followed by a slow depolarization that results in a suprathreshold burst. *C*: graph of membrane potential vs. FSL for this neuron, with a noticeable jump in FSL between −70 and −75 mV. *D*: suprathreshold IN/EX response of a MGD stellate neuron at various membrane potentials. FSL appears to be fixed (↓), regardless of V_{mem}. *E*: example of a burst response in the same neuron at V_{mem} equal to −80 mV. At this hyperpolarized V_{mem}, the $GABA_A$ IPSP is depolarizing and may activate the burst current and then is followed closely by a large EPSP. Overall result is a rapid activation of the Ca^{2+} burst and a short FSL. *F*: graph of membrane potential vs. FSL for the same neuron. FSL does not change over a large voltage range regardless of whether it is in the burst or tonic firing mode. Scale bars in *E* apply to *A*, *B*, *D*, and *E*.

lamic EPSP latency for neurons with IN/EX and EX/O patterns. Nor was there a significant difference in the TRN IPSP latency between any group. Inhibitory TRN inputs consistently had significantly shorter latencies than corticothalamic excitatory inputs (Fig. 8, *A* and *B*, Table 3), indicating that TRN axons conduct faster than corticothalamic axons.

As shown in Fig. 8, *C* and *D*, stimulation of corticothalamic axons generated a graded response, with significantly more discernible levels of excitation (5.8 ± 1.7) than excitatory IC inputs ($P < 0.0001$, Mann-Whitney test). Likewise, blocking glutamatergic transmission using channel blockers APV and DNQX to isolate the GABAergic TRN input revealed multiple amplitude levels for $GABA_A$ and $GABA_B$ IPSPs (4.0 ± 1.4, $n = 5$). The number of amplitude levels for TRN inputs was statistically similar to the number observed for IC IN/O responses. The increases in $GABA_A$ and $GABA_B$ IPSPs paralleled each other, suggesting that single terminals activates both types of GABA receptor postsynaptically. Isolation of TRN inputs with APV and DNQX also illustrated that, like IC inhibitory inputs, descending TRN inputs are monosynaptic to relay neurons (Fig. 8, *E* and *F*).

Pharmacology of descending inputs

Bath application of receptor antagonists confirmed that the short-latency IPSP activated $GABA_A$ receptors ($n = 9$, Fig. 10) and the long-latency IPSP activated $GABA_B$ receptors ($n = 6$, not shown). Like the IC excitatory input, corticothalamic inputs to both types of MGB neurons had distinguishable AMPA and NMDA components with considerable variation in the contribution of each component for individual neurons. NMDA receptor antagonists consistently caused a decrease in the duration of the corticothalamic-evoked EPSP in both MGV (Fig. 9, *A* and *B*) and MGD neurons (Fig. 9*C*) and occasionally decreased the peak amplitude. (Fig. 9*B*). Coapplication of APV and DNQX eliminated the EPSP completely ($n = 5$, Fig. 8*E*). Blocking NMDA receptors produced effects even at membrane potentials (less than −70 mV) where NMDA receptors in other brain regions are blocked by Mg^{2+} ions (Fig. 9, *bottom*). As illustrated in Fig. 9*B*, addition of APV prevented a Ca^{2+} burst activation at −77 mV. Thus the NMDA components of both IC and corticothalamic inputs have an unusual voltage dependence. Furthermore the NMDA component can contribute to the spike response of the burst depolarization.

Timing of suprathreshold corticothalamic responses

Given the modulatory function typically attributed to corticothalamic inputs, it was surprising that suprathreshold responses were evoked in a number of MGB cells by corticothalamic axon stimulation (Figs. 9*C* and 10). Like the suprathreshold responses to the EX/O IC inputs (Fig. 7, *A–C*) and unlike the suprathreshold responses to IN/EX IC inputs (Fig. 7, *D–F*), the latency of the corticothalamic-evoked first spike was dependent on membrane potential, regardless of the presence or absence of a preceding GABAergic event (Fig. 10). Cells of either morphology in both dorsal and ventral divisions could be suprathreshold in response to stimulation of the descending inputs. Figure 10*A* illustrates synaptic and suprathreshold responses to shock stimulation of the descending

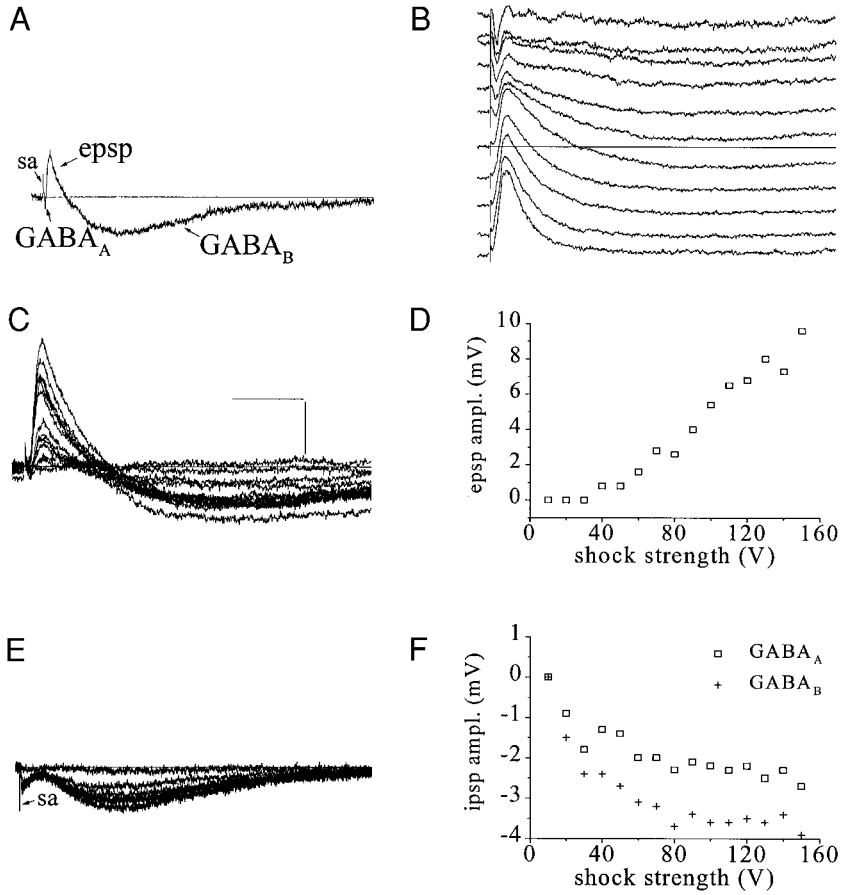

FIG. 8. Representative MGB response to thalamic radiation stimulation. Same neuron was used for *A–D*. *A*: responses of a MGD neuron with the IN/EX response to thalamic radiation stimulation. V_{rest} equals −65 mV. *B*: synaptic response at different membrane potentials on a shorter time scale, illustrating reversal of early $GABA_A$ IPSP. *C*: synaptic responses to increasing shock strength showing increasing EPSP amplitude and indicating that a large number of corticothalamic fibers converge on a single MGB neuron. *D*: graph of peak EPSP amplitude vs. shock intensity with a nearly linear increase in EPSP amplitude as shock strength increases. *E*: responses of a MGD stellate neuron to increasing thalamic radiation stimulation while in APV and DNQX to block excitation. V_{rest} equals −71 mV. *F*: graph of IPSP peak amplitudes at V_{rest} as shock strength increases, indicating the convergence of a small number of TR nucleus (TRN) inputs to MGB neurons and similar thresholds for $GABA_A$ and $GABA_B$ responses. Scale bars in *A* and *E*: $x = 100$ ms, $y = 5$ mV; *B*: $x = 40$ ms, $y = 10$ mV; *C*: $x = 40$ ms, $y = 5$ mV.

input as the cell was moved around rest in normal saline and while the $GABA_A$ IPSP was blocked. In normal saline, at potentials more depolarized than −70 mV, the FSL was fairly consistent, with a typical jitter of 1–2 ms (Fig. 10*B*). Like the spikes generated by excitatory IC inputs in EX/O cells, the FSL of CT-evoked spikes increased as the cell was hyperpolarized due to slow activation of the regenerative Ca^{2+} depolarization. The latency increase and the jitter when hyperpolarized were not significantly affected by the TRN $GABA_A$ IPSP (Fig. 10*B*) because they were unchanged in bicuculline. The inhibitory TRN input did, however, make the production of synaptically evoked spikes less likely at membrane potentials between −55 and −70 mV (Fig. 10).

DISCUSSION

Analysis of MGB morphology

Intracellularly recorded and filled MGV and MGD neurons did not differ in soma size or shape, with pyramidal and round somata of various sizes in both divisions. Similar results were reported recently (Clerici and Coleman 1998) for Nissl-stained rat neurons. In another study, MGD neurons were slightly but significantly smaller than MGV neurons (Senatorov and Hu 1997). Because our results are based on a relatively small number of cells throughout the dorsal and ventral divisions, we may not have been able to detect small divisional differences. However, we reiterate that there were large individual variations in neuron areas without any consistent divisional differences in soma size or shape.

Quantitative analysis of dendritic morphology provided support for described qualitative differences in MGB cell morphology (Clerici et al. 1990; Morest 1984), and a way to distinguish tufted from stellate neurons. Such a quantitative analysis allowed a more objective correlation of morphology with physiology and location for individual cells. Tufted neurons in the MGV and MGD had shorter dendrites, a smaller dendritic tree area, more profuse branching, and greater dendritic orientation compared with stellate neurons, which were only found in MGD. In contrast to other anatomic studies (Clerici and Coleman 1990; Hu et al. 1994; Morest 1964, Morest 1965a; Winer and Morest 1983) most of our labeled neurons were recorded and drawn in the horizontal plane because we wanted to drive synaptic inputs. However, we recorded from and drew a small number of neurons from coronal and sagittal slices and observed no differences in quantitative dendritic characteristics. Although tufted neuron dendrites were significantly more polarized than stellate dendrites, they were not as strongly polarized as Golgi studies of rat and cat have suggested. A lack of polarization was most evident at <50 μm from the soma, where tufted neuron dendrites sometimes projected in all directions. One reason that we observed longer dendrites and less oriented dendritic trees may be that we analyzed single cells from relatively thick sections (400–500 μm). A previous rat Golgi study used 100- to 150-μm sections (Clerici et al. 1990) and labeling of many neurons in each section restricts analysis of dendrites to single sections. Such restrictions could omit significant portions of the dendritic tree found in adjacent sections. Anatomical stud-

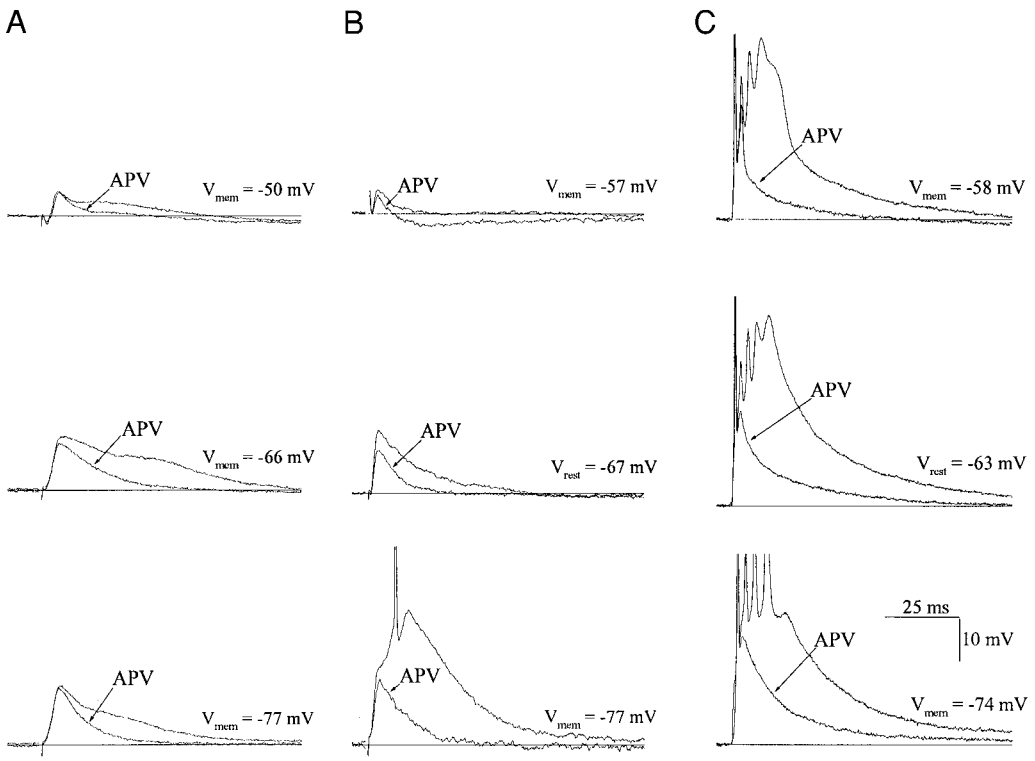

FIG. 9. Effect of NMDA receptor blockade on corticothalamic excitation. Responses of 3 neurons (*A–C*) to shocks applied to the thalamic radiations as the membrane potential is held above −60 mV (*top*), close to −65 mV (*middle*), and below −70 mV (*bottom*). ↓, traces recorded during APV application, other traces taken in normal saline. *A*: example of a MGV tufted neuron with only a modest NMDA component that is still present at −77 mV (*bottom*). *B*: responses from an MGV tufted cell illustrating a neuron that requires the NMDA component to generate a Ca^{2+} burst at −77 mV (*bottom*). *C*: recordings from a MGD neuron with a strong NMDA component. NMDA component is necessary to produce a response with multiple spikes. Action potentials in *B* and *C* were truncated. Scale bars in *C* (*bottom*) apply to all traces.

ies support the existence of laminae in MGV (Clerici and Coleman 1990; Morest 1965a), which are thought to be the anatomic substrate of isofrequency laminae recorded in vivo (Aitkin and Webster 1971, 1972). Although the MGV may have cell laminae and numerous neurons with dendrites projecting parallel to those laminae, the overlap of inputs received by neurons in adjacent laminae is probably substantial on dendrites that project orthogonally to the laminae. In the rat, dendritic tree orientation may not be as significant a factor in contributing to the narrow frequency response as long as the proximal dendrites lie within a single cell lamina.

Differences in the dendritic characteristics of tufted and stellate neurons resemble some of those described for cells in visual and somatosensory thalamus. Somatosensory neurons in the rat medial division of the posterior thalamic group and ventrobasal complex had different morphologies but responded similarly to tactile input (OHara and Havton 1994). In contrast, cat dorsal LGN (dLGN) neurons have anatomic features that are correlated fairly well with their visual responses (Friedlander et al. 1981; Humphrey and Weller 1988), including specialized dendritic appendages that are involved in triadic synapses with interneurons. Rat MGB neurons lack such specialized dendritic appendages and are more similar to rat somatosensory neurons. The morphological differences between tufted and stellate MGB cells may reflect differences in how afferents converge on them, but it is hard to know whether this would cause PSPs to integrate differently to affect acoustic response properties.

Intrinsic properties

Overall, the membrane characteristics we observed were similar to those reported for a handful of neurons in medial geniculate and a very large number of neurons in other thalamic regions (Crunelli et al. 1987; Jahnsen and Llinas 1984a,b; Pape and McCormick 1995; Turner et al. 1997). However, in contrast to the previous results described from the MGB (Hu 1995; Hu et al. 1994; Senatorov and Hu 1997), we found that identified neurons in the ventral and dorsal divisions of the MGB have similar intrinsic properties, with only a few consistent differences (Table 2). Furthermore these properties were not segregated by cell morphology. The main difference in intrinsic properties was an increased prevalence of a sag potential in MGV cells. This sag was the only intrinsic property correlated with morphology. Only tufted neurons, which included MGV and some MGD cells, displayed a sag, but not all tufted neurons displayed a sag.

A discussion of the possible discrepancies between our results and those of the only other studies comparing intracellular characteristics of MGV and MGD neurons is warranted because those studies have implied that differences in intrinsic features could account for the nature of the different responses to auditory stimuli seen in vivo when recording from dorsal versus ventral division cells (Hu 1995; Hu et al. 1994). One possible explanation for some of the differences is the $[K^+]$ of the salines, which has a controlling influence on resting membrane potential. However, changing our $[K^+]$ to match that of

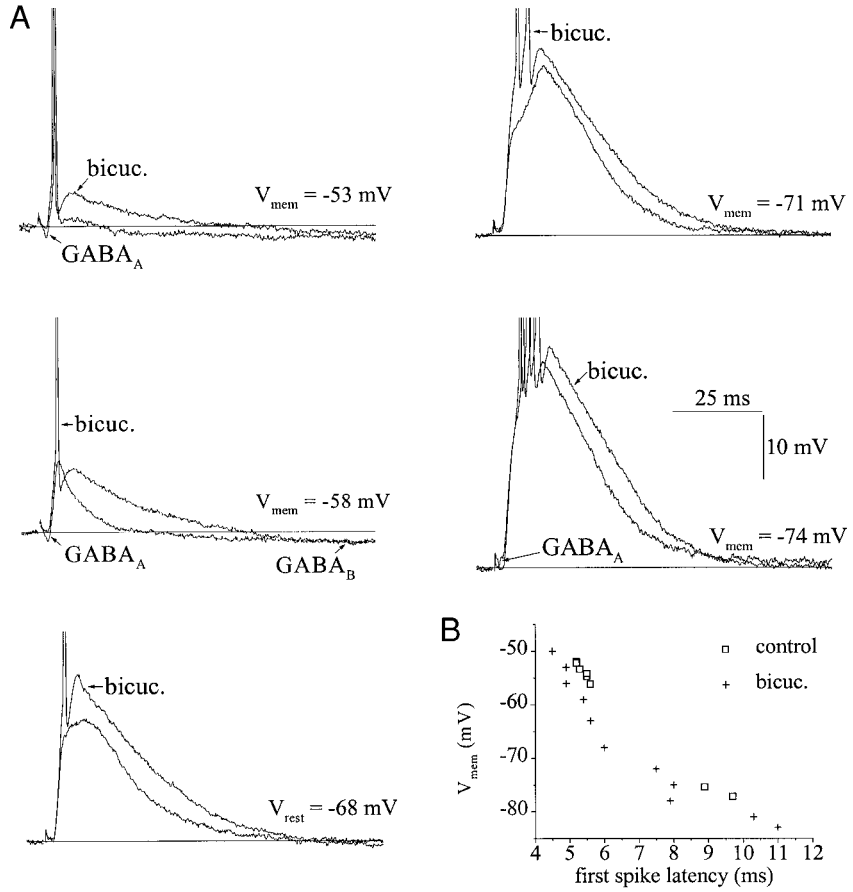

FIG. 10. Sensitivity of corticothalamic-evoked FSL to V_{mem} and the effect of TRN $GABA_A$ receptor blockade. *A*: responses of a MGV tufted neuron matched for DC level, in normal saline and saline with bicuculline (bicuc.), as the membrane potential was moved around rest. ←, traces recorded during bicuculline application. FSL increases with hyperpolarization even in normal saline with an intact TRN $GABA_A$ IPSP. Corticothalamic EPSPs become suprathreshold between −58 and −71 mV when $GABA_A$ IPSPs are blocked, potentials that were subthreshold in normal saline. *B*: graph of FSL vs. V_{mem} in control and in bicuculline (bicuc.). Under both conditions the corticothalamic-evoked FSL increases rapidly over a small voltage range at hyperpolarized V_{mem}. Action potentials in *A* were truncated. Scale bar in *A* (*bottom right*) applies to all traces.

the previous studies did not create populations of MGB neurons that were resolvable by resting potential, firing mode, or subdivision nor did it alter our finding that both MGV tufted and MGD stellate and tufted neurons could be in burst or tonic mode.

A second possible explanation for the differences could be the type of preparation used. Our recordings were done in a 400- to 500-μm slice taken in any of the three standard planes and from cells in all regions of the dorsal and ventral divisions. Hu and colleagues used an ''explant'' preparation (Hu 1995; Hu et al. 1994), where a portion of the unilateral diencephalon containing the entire brachium of the IC and medial geniculate was removed and isolated. With this preparation, they only recorded from the caudal two-thirds to three-quarters of the MGB because rostral MGB is obscured by the lateral geniculate nucleus and the brachium of the superior colliculus (Paxinos and Watson 1986) and only sampled cells $\leq$400–500 μM deep to the free surface of the MGB. Thus access was restricted to the caudodorsal MGD and the caudal portion of the latero-ventral division of the MGV (Clerici and Coleman 1990). Such an explant preparation would leave more MGB circuitry intact, but it is not clear whether structures deeper than 400–500 μM would still be viable. When we restricted our analysis to those neurons that are accessible in the explant preparation, we still found that MGV and MGD neurons had similar membrane characteristics except for the increased percentage of MGV neurons expressing a sag. Therefore differences in the regions sampled do not appear to cause the conflicting results. In addition, differences in morphology were not correlated with differences in membrane properties because a comparison of identified MGV tufted and MGD stellate neurons yielded identical results to the full populations of MGV and MGD neurons.

Another possible explanation is in the choice of experimental data. By comparing a selected subset of MGV cells that were in single spike mode and MGD cells that were in burst mode, a mean resting membrane potential that was 9 mV more negative in MGD cells was noted (Hu 1995). We also note a similar difference in membrane potential when comparing bursting versus tonic firing neurons (see RESULTS). However, our data taken from all sampled cells do not show such a difference in membrane potential between areas or between cell types. Because 20–30% of MGV neurons in the explant preparation were in the burst firing mode (Hu et al. 1994), similar to the proportion found in our study (Table 2), exclusion of MGV bursting neurons when comparing MGV and MGD resting potentials may have made the populations appear more segregated than the total population of MGV and MGD neurons. Using sharp microelectrodes, the difference in potentials was attributed to the presence of a Cs^+-sensitive sag potential (I_h) found only in MGV neurons that was active at resting potential (Hu 1995). We also have found the sag mainly in MGV neurons, but our data indicate that tufted cells in MGD also can display a sag potential. A whole cell recording study also found enhanced activity of Na^+-K^+-ATPase in MGD neurons relative to MGV neurons (Senatorov and Hu 1997). However, using sharp microelectrodes, the small divisional difference in Na^+-K^+-ATPase currents would not contribute to a significant difference in resting potentials. Regardless of cell

morphology or location in the MGB, synaptic stimulation of neurons in the present study could evoke bursts at hyperpolarized membrane potentials and one or more Na^+ spikes at depolarized potentials. Together these data would bring into question the notion that membrane potential, controlled by intrinsic features of cells in dorsal versus ventral MGB, is a controlling influence in response differences seen in vivo.

Thus in vivo, synaptic control of resting membrane potential is probably a more powerful determinant of neuronal response than intrinsic properties. Rat thalamic neurons receive cholinergic inputs from the laterodorsal tegmentum and pedunculopontine nucleus and noradrenergic inputs from the locus coeruleus (McCormick 1992). Both of these modulatory pathways would be preserved in the explant preparation but not in the slice preparation, but the nuclei are also deep enough that they might be adversely affected in the explant. Mooney et al. (1995) indicated that MGV neurons were depolarized out of the burst range by application of muscarinic acetylcholine receptor agonists, whereas MGD neurons were hyperpolarized. In addition, activation of α-adrenoreceptors in thalamocortical neurons can cause depolarization, whereas β-adrenoreceptors also can cause depolarization by a positive shift in the activation curve of I_h (McCormick 1992). Because the difference between MGD and MGV neuron resting potentials in the explant preparation was due to the strong activation of I_h in MGV tufted neurons, it is possible that selective activation of β-adrenoreceptors was able to cause the observed differences in resting potential. Until an in vivo MGB intracellular recording study is done, we cannot know whether MGB neurons normally are maintained at different membrane potentials. Such a study also would help to determine the cause(s) of the increased latency of MGD neuron responses to sound, such as a long-latency Ca^{2+} burst (Hu 1995; Hu et al. 1994) or the use of suboptimal acoustic stimuli to activate MGD neurons.

Inputs from the IC

BIC stimulation elicited excitatory and inhibitory synaptic events in MGV and MGD neurons, and we have shown previously (Peruzzi et al. 1997) that they arise from monosynaptic IC inputs. Here we analyze the relationship of the inhibitory and excitatory IC projections. BIC stimulation most commonly elicited IN/EX or EX/O responses, but EX/IN and IN/O responses also were evoked. Both MGV and MGD displayed similar proportions of response combinations, but throughout the MGB, suprathreshold EX/O responses were only observed in neurons with tufted morphology. Increased synaptic amplitudes with increased shock intensity to BIC fibers implies that IC excitatory and inhibitory PSPs often result from convergence of a small number of inputs. Analysis of PSP latencies implied that there are excitatory and inhibitory IC axons that conduct at different rates. Pharmacological blockade of $GABA_A$ IPSPs did not change the EPSP latency for IN/EX or EX/IN inputs, implying that the excitatory fibers generating EX/O patterns may be a different population than those producing IN/EX patterns. Although this analysis cannot predict the interaction of inputs that produces variable response latencies to sound observed in vivo, it can provide some insight into the response combinations and relative timings of inputs necessary to produce the in vivo responses. The latency of IN/EX EPSPs was significantly longer than the latency of EX/O EPSPs, and the latency of IN/EX, IN/O, and MGV EX/IN $GABA_A$ IPSPs was significantly shorter than the latency of MGD EX/IN IPSPs. Anatomic evidence from cat (St. Marie et al. 1997) has shown that a variety of sizes of both GABAergic and non-GABAergic (presumably glutamatergic) fibers run in the BIC that are thought to arise primarily from IC cells. Only a small percentage of medium and small IC axons were GABAergic, but about half of the large diameter IC axons were. Thus it is probably not surprising that different EPSP and IPSP latencies are observed and that the IPSPs often preceded EPSPs. It is also probably not surprising, given the fairly large population of small non-GABAergic axons reported that many EPSPs are small and subthreshold. Taken together, these results support the notion that IC inhibition can be fast and may precede excitation under some conditions in vivo. Certain neurons in the awake mustached bat IC display significant facilitation when a CF pulse and its doppler-shifted echo are presented together compared with either stimulus presented alone (Suga et al. 1997). This effect was enhanced by bicuculline iontophoresis, largely due to an increase in an APV-sensitive late component (Suga et al. 1997). Blockade of $GABA_A$ inhibition in our slices could uncover a robust suprathreshold IC input with a significant APV sensitive late component (Fig. 6, *D* and *E*).

Pharmacological analysis showed that excitatory IC inputs activated AMPA and NMDA glutamate receptors and inhibitory IC inputs activated $GABA_A$ and $GABA_B$ receptors. The NMDA component was active even at hyperpolarized membrane potentials and could affect the MGB cell's ability to respond with a Ca^{2+} burst (Fig. 6*E*). Many of the IC EPSP properties described here have been observed in the MGB and other thalamic regions. Previous studies of rat MGB, LGN, and ventrobasal complex (VB) neurons showed that stimulation of ascending inputs to these regions evokes EPSPs with AMPA and NMDA components (Hu et al. 1994; Kao and Coulter 1997; Turner et al. 1994). In the MGB, it was reported that IC EPSPs in MGV neurons were largely due to AMPA receptor activation, whereas those in MGD had a more equal mixture of AMPA and NMDA components (Hu et al. 1994). Although we did not investigate this issue in detail, our results indicate that there are clear exceptions (Fig. 6*A*) and that the proportion of each component may vary between neurons. Further study is required to determine the extent of this variability and whether the proportion of AMPA and NMDA components is related to the MGB response pattern to IC input observed in the slice.

Like the present study, studies of the rat and cat dorsal LGN showed a noticeable NMDA component, even at hyperpolarized membrane potentials < -75 mV, that was occasionally necessary to evoke a Ca^{2+} burst in response to optic tract stimulation (Esguerra et al. 1992; Turner et al. 1994). In these LGN neurons, the NMDA component expanded the voltage range of the burst. NMDA antagonists applied to the cat LGN in vivo could reduce the visual responses of X and Y neurons (Hartveit and Heggelund 1990; Heggelund and Hartveit 1990; Kwon et al. 1992). The functional role of the IC NMDA component in the MGB is unclear because the effects of NMDA receptor agonists or antagonists on MGB neurons in vivo have not been investigated in detail (Suga et al. 1997).

In agreement with a previous MGB study (Hu 1995) we found that, for most cells with suprathreshold IC input, the latency of the BIC-evoked first spike was dependent on mem-

brane potential and EPSP height. In our study, suprathreshold burst responses at hyperpolarized membrane potentials were observed mainly in neurons not receiving inhibitory IC input (EX/O input). When depolarized, evoked action potentials were short latency and consistent, but hyperpolarization below −70 mV greatly increased the FSL over a small voltage range probably because of activation of the regenerative Ca^{2+} burst and the increased time for the burst to reach spike threshold. If neurons with EX/O inputs actually receive little or no IC inhibition in vivo, then a burst response may be useful for the amplification and detection of weak stimuli, which would not require temporal precision. Receiver operating characteristics analysis of cat LGN cells has shown that the burst mode is suited for signal detection (Guido et al. 1995) and that LGN neurons can burst during waking, especially during the initial fixation to a visual stimulus (Guido and Weyand 1995). The nonlinear increase in FSL with hyperpolarization and its interplay with EPSP height makes it unlikely that the burst response is an analogue to temporal converter (Hu 1995) because multiple combinations of EPSP height and membrane potential could produce the same FSL.

We noted that some neurons with inhibitory IC inputs could fire short-latency action potentials at more depolarized membrane potentials, usually greater than −55 mV, and in two cases, the neurons responded over a wide range of membrane potentials both above and below rest. For these two neurons, the FSL was independent of membrane potential. The unusual short-latency response at hyperpolarized potentials appeared to be caused by the combination of depolarizing inhibition rapidly activating the Ca^{2+} burst followed closely by a large excitatory input. Moreover, responses at different membrane potentials may converge to produce a more uniform starting point on which the EPSP is superimposed. Further experiments are necessary to determine whether blocking inhibition will abolish the fixed FSL and whether the IPSP and EPSP latencies affects the timing consistency. However, because block of $GABA_A$ receptors in two neurons with IC inhibition revealed poorly timed suprathreshold responses (Fig. 6, *D* and *E*), the early IPSP probably has a significant role in generating well-timed first spikes. In the LGN, consistently timed spikes are associated with the tonic firing mode, a state believed to be suited for signal analysis (Guido et al. 1995). Because these IN/EX cells seem to be combining signal amplification and detection capabilities provided by the burst mode with the consistently timed spikes useful for signal analysis, it implies that they may be able to consistently analyze weak acoustic stimuli.

Inputs from the cortex and the thalamic reticular nucleus

Stimulation of the thalamic radiations excited corticothalamic and TRN fibers, causing an IN/EX response in most neurons. Overall, the corticothalamic excitatory input had more distinguishable amplitude levels than IC input as the stimulus intensity increased, implying that more corticothalamic fibers converge onto single MGB neurons. Like the ascending IC input, the excitatory corticothalamic inputs activated AMPA and NMDA receptors, whereas the inhibitory TRN inputs activated $GABA_A$ and $GABA_B$ receptors. The NMDA component of the corticothalamic excitatory input also had an unusual voltage dependence with a detectable APV-sensitive component even at membrane potentials below −70 mV. Like the EX/O IC input, the FSL of corticothalamic action potentials was sensitive to membrane potential, regardless of whether TRN inhibition was present.

Although this is the first intracellular description of descending input to MGB neurons, studies in other thalamic regions have investigated the corticothalamic and TRN inputs. Stimulation of the internal capsule or cortex causes a combination of EPSPs and IPSPs in somatosensory, motor, and anterior thalamic regions (Deschenes and Hu 1990; Kao and Coulter 1997; Pare et al. 1991; Warren et al. 1994). In these studies, the EPSP usually preceded the IPSP. We showed that the IPSP consistently preceded the EPSP. This discrepancy is probably due to the different placement of the stimulating electrodes. Placement in the cortex or internal capsules would necessitate synaptic activation of TRN neurons that then would project to thalamic neurons. Our placement in the thalamic radiations directly activated TRN axons. Our responses suggest that TRN axons conduct faster than most corticothalamic axons. Isolated corticothalamic inputs in other thalamic regions were shown to be composed of many smaller events (Deschenes and Hu 1990; Warren et al. 1994), similar to our results for MGB neurons.

Stimulation of the descending inputs in other thalamic areas also has been shown to activate AMPA and NMDA receptors via cortical input and $GABA_A$ and $GABA_B$ receptors via TRN input. $GABA_A$ receptor blockade or destruction of the TRN resulted in substantial increases in EPSP amplitude that could uncover a suprathreshold response (Deschenes and Hu 1990; Eaton and Salt 1996; Warren et al. 1994), an effect that we also have observed (Fig. 10*A*). In these studies, the NMDA contribution to the corticothalamic EPSP ranged from moderate (Deschenes and Hu 1990; Eaton and Salt 1996), which was observed most often in the present study (Fig. 9), to dominant (Kao and Coulter 1997). Voltage-clamp analysis of cortical inputs to rat VB neurons revealed substantial NMDA currents between −50 and −80 (Kao and Coulter 1997). One possible explanation is that NR2C and NR2D NMDA receptor subunits are resistant to Mg^{2+} block at physiological resting potentials and are present in the thalamus of young and adult rats (Kao and Coulter 1997; Monyer et al. 1994; Wenzel et al. 1995, 1997). It is notable that both the IC and cortical inputs appear to have similar unusual NMDA channel voltage dependence, suggesting that both inputs may activate postsynaptic NMDA receptors with similar subunit compositions.

Electrical stimulation of corticothalamic inputs can elicit suprathreshold responses in vitro and in vivo (Deschenes and Hu 1990; Kao and Coulter 1997; this study), implying that these inputs could drive sensory responses of thalamocortical neurons. This suggestion opposes the simply modulatory role normally attributed to the corticothalamic input's function (Crick and Koch 1998; McCormick and Bal 1994). Although electrical stimulation produces artificially synchronous activation of corticothalamic axons, cortical inputs appear to generate suprathreshold events in ventrolateral nucleus neurons during cortical ''desynchronization'' in anesthetized cats (Steriade 1997). During desynchronization, the cortical excitation of TRN neurons appeared to be generally weak (Steriade 1997), unlike the strong corticoreticular input during sleep spindles and delta rhythms (Contreras and Steriade 1996; Contreras et al. 1996; Destexhe et al. 1998; Steriade 1997). A class of possibly interconnected corticothalamic neurons has been iden-

tified in the cat cortex that fires rhythmic high-frequency bursts at 20–50 Hz (Steriade et al. 1998), which might be able to quickly synchronize corticothalamic neurons and provide a strong excitatory corticothalamic input. Another characteristic of inputs considered to be drivers is that they determine the receptive field of the postsynaptic cell. In the mustached bat MGB, focal inactivation of auditory cortex produced a best frequency (BF) shift for cells the BF of which was slightly different from the inactivated region of cortex (Zhang et al. 1997). Finally, cortex-dependent input can generate activity in some cat MGB cells for hundreds of milliseconds after the offset of acoustic stimulation, suggesting that cortical input may cause action potentials in MGB neurons in the absence of IC activity (Ryugo and Weinberger 1976).

The inhibitory TRN input was present in most MGB neuron responses, and multiple fibers appeared to converge onto a single MGB neuron (Fig. 8, *E* and *F*). Pharmacological blockade of TRN IPSPs invariably increased the corticothalamic EPSP and could decrease the stimulus intensity necessary to evoke a spike or increase the ability to spike over a greater voltage range (Fig. 9*A*). Although the FSL increased as membrane potential decreased, which also occurred for EX/O IC inputs, TRN inhibition had little effect on the corticothalamic evoked FSL (Fig. 10). Thus TRN inhibition may not be as strongly coupled to corticothalamic excitation as IC inhibition is to IC excitation. It is also possible that TRN inhibition could be associated more closely with ascending IC excitation because TRN activation preceding click stimuli could suppress the click response in rat MGB neurons for 20–30 ms (Shosaku and Sumitomo 1983).

Correlation of MGB anatomy and physiology

In support of the hypothesis that the dendritic architecture of MGB neurons does not predict their in vivo responses, we found only a few consistent differences between tufted and stellate neurons physiologically in vitro. Only tufted neurons displayed a depolarizing sag, as reported in previous studies (Hu 1995). Because we found that the resting potential of tufted and stellate neurons was similar, the significance of the sag in tufted neurons is unclear. Perhaps the resting potential of tufted neurons can be modulated by changing the voltage dependence of the sag activation by modulatory neurotransmitters (Banks et al. 1993; Pape and McCormick 1989), the sag curtails the inhibitory duration of $GABA_B$ inhibition, or it promotes a more robust rebound burst after hyperpolarization (Luthi and McCormick 1998). The latter hypothesis is less likely because we did not observe an enhanced burst frequency or number of spikes in MGV neurons compared with MGD neurons.

Only a subset of tufted neurons were capable of responding to BIC stimulation with a large all-or-none EPSP that was often suprathreshold. These EPSPs may be the physiological equivalent of large excitatory afferents observed at the light and electron microscopic levels in the cat and hamster (Campbell and Frost 1988; Jones and Rockel 1971; Majorossy and Kiss 1976) and at the light level in ferret and guinea pig (Malmierca et al. 1997; Pallas and Sur 1994). It is possible that MGD tufted neurons receiving this large excitatory input are those that project to layer IV of primary auditory cortex (Mitani et al. 1987). Such a projection would blur the classification of MGV as a lemniscal or first-order thalamic nucleus and MGD as an extralemniscal or higher-order thalamic nucleus (Guillery 1995). Finally, one of the neurons with a fixed FSL at all potentials had stellate morphology and was found in the MGD. The general lack of correlation of morphology or MGB subdivision with intrinsic physiology implies that most MGB neurons can perform a similar spectrum of transformations of synaptic input. It further indicates that MGB acoustic responses are dictated mainly by the combination and pattern of synaptic inputs that MGB neurons receive. Future studies should investigate whether MGB neurons might receive specific combinations of input designed to process particular stimulus features. One might expect that neurons receiving EX/O IC inputs would process inputs in a manner similar to LGN or VB neurons receiving EX/O retinal or trigeminal input, but MGB neurons receiving IN/EX inputs might have more complex responses reflecting their unique pattern of innervation from ascending inputs.

We are indebted to J. Ekleberry, J. Meister, and I. Siggelkow for excellent technical assistance. We thank D. Uhlrich and R. Guillery for helpful comments on a draft of the manuscript and W. Rhode for the use of his Neurolucida system.

This work was supported by the National Institute on Deafness and Other Communications Disorders Grant DC-00116 and funds provided by a grant to the University of Wisconsin Medical School from the Howard Hughes Medical Institute Research Resources Program for Medical Schools.

Address for reprint requests: P. H. Smith, Dept. of Anatomy, University of Wisconsin-Madison, Madison, WI 53706-1532.

Received 24 August 1998; accepted in final form 13 January 1999.

REFERENCES

ADAMS, J. C. Heavy metal intensification of DAB-based HRP reaction product. *J. Histochem. Cytochem.* 29: 775, 1981.

AGHAJANIAN, G. K. AND RASMUSSEN. Intracellular studies in the facial nucleus illustrating a simple new method for obtaining viable motor neurons in adult rat brain slices. *Synapse* 3: 331–338, 1989.

AITKIN, L. M. AND PRAIN, S. M. Medial geniculate body: unit responses in the awake cat. *J. Neurophysiol.* 37: 512–521, 1974.

AITKIN, L. M. AND WEBSTER, W. R. Tonotopic organization in the medial geniculate body of the cat. *Brain Res.* 26: 402–405, 1971.

AITKIN, L. M. AND WEBSTER, W. R. Medial geniculate body of the cat: organization and responses to tonal stimuli of neurons in ventral division. *J. Neurophysiol.* 35: 365–380, 1972.

ALLON, N., YESHURUN, Y., AND WOLLBERG, Z. Responses of single cells in the medial geniculate body of awake squirrel monkeys. *Exp. Brain Res.* 41: 222–232, 1981.

ANDERSEN, R. A., ROTH, G. L., AITKIN, L. M., AND MERZENICH, M. M. The efferent projections of the central nucleus and the pericentral nucleus of the inferior colliculus in the cat. *J. Comp. Neurol.* 194: 649–662, 1980.

BAJO, V. M., ROUILLER, E. M., WELKER, E., CLARKE, S., VILLA, A. E., DE RIBAUPIERRE, Y., AND DE RIBAUPIERRE F. Morphology and spatial distribution of corticothalamic terminals originating from the cat auditory cortex. *Hear. Res.* 83: 161–174, 1995.

BANKS, M. I., PEARCE, R. A., AND SMITH, P. H. Hyperpolarization-activated cation current (I_h) in neurons of the medial nucleus of the trapezoid body: voltage clamp analysis and enhancement by norepinephrine and cAMP suggest a modulatory mechanism in the auditory brainstem. *J. Neurophysiol.* 70: 1420–1432, 1993.

BORDI, F. AND LEDOUX, J. E. Response properties of single units in areas of rat auditory thalamus that project to the amygdala. I. Acoustic discharge patterns and frequency receptive fields. *Exp. Brain Res.* 98: 261–274, 1994.

BOURASSA, J. AND DESCHENES, M. Corticothalamic projections from the primary visual cortex in rats: a single fiber study using biocytin as an anterograde tracer. *Neuroscience* 66: 253–263, 1995.

BOURASSA, J., PINAULT, D., AND DESCHENES, M. Corticothalamic projections from the cortical barrel field to the somatosensory thalamus in rats: a

single-fibre study using biocytin as an anterograde tracer. *Eur. J. Neurosci.* 7: 19–30, 1995.

CALFORD, M. B. The parcellation of the medial geniculate body of the cat defined by the auditory response properties of single units. *J. Neurosci.* 3: 2350–2364, 1983.

CALFORD, M. B. AND AITKIN, L. M. Ascending projections to the medial geniculate body of the cat: evidence for multiple, parallel auditory pathways through thalamus. *J. Neurosci.* 3: 2365–2380, 1983.

CALFORD, M. B. AND WEBSTER, W. R. Auditory representation within principal division of cat medial geniculate body: an electrophysiology study. *J. Neurophysiol.* 45: 1013–1028, 1981.

CAMPBELL, G. AND FROST, D. O. Synaptic organization of anomalous retinal projections to the somatosensory and auditory thalamus: target-controlled morphogenesis of axon terminals and synaptic glomeruli. *J. Comp. Neurol.* 272: 383–408, 1988.

CLAREY, J. C., BARONE, P., AND IMIG, T. J. Physiology of thalamus and cortex. In: *The Mammalian Auditory Pathway: Neurophysiology*, edited by A. N. Popper and R. R. Fay. New York: Springer-Verlag, 1992, p. 232–334.

CLERICI, W. J. AND COLEMAN, J. R. Anatomy of the rat medial geniculate body. I. Cytoarchitecture, myeloarchitecture, and neocortical connectivity. *J. Comp. Neurol.* 297: 14–31, 1990.

CLERICI, W. J. AND COLEMAN, J. R. Postnatal cytoarchitecture of the rat medial geniculate body. *J. Comp. Neurol.* 399: 110–124, 1998.

CLERICI, W. J., MCDONALD, A. J., THOMPSON, R., AND COLEMAN, J. R. Anatomy of the rat medial geniculate body. II. Dendritic morphology. *J. Comp. Neurol.* 297: 32–54, 1990.

CONTRERAS, D., DESTEXHE, A., SEJNOWSKI, T. J., AND STERIADE, M. Control of spatiotemporal coherence of a thalamic oscillation by corticothalamic feedback. *Science* 274: 771–774, 1996.

CONTRERAS, D. AND STERIADE, M. Spindle oscillation in cats: the role of corticothalamic feedback in a thalamically generated rhythm [published erratum] *J. Physiol. (Lond.)* 490: 159–179, 1996.

CRABTREE, J. W. Organization in the auditory sector of the cat's thalamic reticular nucleus. *J. Comp. Neurol.* 390: 167–182, 1998.

CRICK, F. AND KOCH, C. Constraints on cortical and thalamic projections: the no-strong-loops hypothesis. *Nature* 391: 245–250, 1998.

CRUNELLI, V., KELLY, J. S., LERESCHE, N., AND PIRCHIO, M. The ventral and dorsal lateral geniculate nucleus of the rat: intracellular recordings in vitro. *J. Physiol. (Lond.).* 384: 587–601, 1987a.

CRUNELLI, V., LERESCHE, N., AND PARNAVELAS, J. G. Membrane properties of morphologically identified X and Y cells in the lateral geniculate nucleus of the cat in vitro. *J. Physiol. (Lond.).* 390: 243–256, 1987b.

DESCHENES, M. AND HU, B. Electrophysiology and pharmacology of the corticothalamic input to lateral thalamic nuclei: an intracelluar study in the cat. *Eur. J. Neurosci.* 2: 140–152, 1990.

DESTEXHE, A., CONTRERAS, D., AND STERIADE, M. Mechanisms underlying the synchronizing action of corticothalamic feedback through inhibition of thalamic relay cells. *J. Neurophysiol.* 79: 999–1016, 1998.

EATON, S. A. AND SALT, T. E. Role of *N*-methyl-D-aspartate and metabotropic glutamate receptors in corticothalamic excitatory postsynaptic potentials in vivo. *Neuroscience* 73: 1–5, 1996.

ESGUERRA, M., KWON, Y. H., AND SUR, M. Retinogeniculate EPSPs recorded intracellularly in the ferret lateral geniculate nucleus in vitro: role of NMDA receptors. *Vis. Neurosci.* 8: 545–555, 1992.

FRIEDLANDER, M. J., LIN, C. S., STANFORD, L. R., AND SHERMAN, S. M. Morphology of functionally identified neurons in lateral geniculate nucleus of the cat. *J. Neurophysiol.* 46: 80–129, 1981.

GILBERT, C. D. AND KELLY, J. P. The projections of cells in different layers of the cat's visual cortex. *J. Comp. Neurol.* 163: 81–105, 1975.

GUIDO, W., LU, S. M., VAUGHAN, J. W., GODWIN, D. W., AND SHERMAN, S. M. Receiver operating characteristic (ROC) analysis of neurons in the cat's lateral geniculate nucleus during tonic and burst response mode. *Vis. Neurosci.* 12: 723–741, 1995.

GUIDO, W. AND WEYAND, T. Burst responses in thalamic relay cells of the awake behaving cat. *J. Neurophysiol.* 74: 1782–1786, 1995.

GUILLERY, R. W. Anatomical evidence concerning the role of the thalamus in corticocortical communication: a brief review. *J. Anat.* 187: 583–592, 1995.

HARTVEIT, E. AND HEGGELUND, P. Neurotransmitter receptors mediating excitatory input to cells in the cat lateral geniculate nucleus. II. Nonlagged cells. *J. Neurophysiol.* 63: 1361–1372, 1990.

HEGGELUND, P. AND HARTVEIT, E. Neurotransmitter receptors mediating excitatory input to cells in the cat lateral geniculate nucleus. I. Lagged cells. *J. Neurophysiol.* 63: 1347–1360, 1990.

HOOGLAND, P. V., WELKER, E., AND VAN DER LOOS, H. Organization of the projections from barrel cortex to thalamus in mice studied with Phaseolus vulgaris-leucoagglutinin and HRP. *Exp. Brain Res.* 68: 73–87, 1987.

HOOGLAND, P. V., WOUTERLOOD, F. G., WELKER, E., AND VAN DER LOOS, H. Ultrastructure of giant and small thalamic terminals of cortical origin: a study of the projections from the barrel cortex in mice using Phaseolus vulgaris leuco-agglutinin (PHA-L). *Exp. Brain Res.* 87: 159–172, 1991.

HU, B. Cellular basis of temporal synaptic signalling: an in vitro electrophysiological study in rat auditory thalamus. *J. Physiol. (Lond.)* 483: 167–182, 1995.

HU, B., SENATOROV, V., AND MOONEY, D. Lemniscal and non-lemniscal synaptic transmission in rat auditory thalamus. *J. Physiol. (Lond.)* 479: 217–231, 1994.

HUMPHREY, A. L. AND WELLER, R. E. Structural correlates of functionally distinct X-cells in the lateral geniculate nucleus of the cat. *J. Comp. Neurol.* 268: 448–468, 1988.

IMIG, T. J. AND MOREL, A. Tonotopic organization in ventral nucleus of medial geniculate body in the cat. *J. Neurophysiol.* 53: 309–340, 1985.

IRVINE, D. R. Physiology of the auditory brainstem. In: *The Mammalian Auditory Pathway: Neurophysiology*, edited by R. R. Fay and A. N. Popper. New York: Springer-Verlag, 1992, p. 152–231.

JAHNSEN, H. AND LLINAS, R. Ionic basis for the electro-responsiveness and oscillatory properties of guinea-pig thalamic neurones in vitro. *J. Physiol. (Lond.)* 349: 227–247, 1984a.

JAHNSEN, H. AND LLINAS, R. Electrophysiological properties of guinea-pig thalamic neurones: an in vitro study. *J. Physiol. (Lond.)* 349: 205–226, 1984b.

JONES, E. G. Some aspects of the organization of the thalamic reticular complex. *J. Comp. Neurol.* 162: 285–308, 1975.

JONES, E. G. AND POWELL, T. P. An electron microscopic study of the mode of termination of cortico-thalamic fibres within the sensory relay nuclei of the thalamus. *Proc. R. Soc. Lond. B Biol. Sci.* 172: 173–185, 1969a.

JONES, E. G. AND POWELL, T. P. Electron microscopy of synaptic glomeruli in the thalamic relay nuclei of the cat. *Proc. R. Soc. Lond. B Biol. Sci.* 172: 153–171, 1969b.

JONES, E. G. AND ROCKEL, A. J. The synaptic organization in the medial geniculate body of afferent fibres ascending from the inferior colliculus. *Z. Zellforsch. Mikrosk. Anat.* 113: 44–66, 1971.

KAO, C. Q. AND COULTER, D. A. Physiology and pharmacology of corticothalamic stimulation-evoked responses in rat somatosensory thalamic neurons in vitro. *J. Neurophysiol.* 77: 2661–2676, 1997.

KUDO, M. AND NIIMI, K. Ascending projections of the inferior colliculus onto the medial geniculate body in the cat studied by anterograde and retrograde tracing techniques. *Brain Res.* 155: 113–117, 1978.

KUDO, M. AND NIIMI, K. Ascending projections of the inferior colliculus in the cat: an autoradiographic study. *J. Comp. Neurol.* 191: 545–556, 1980.

KWON, Y. H., NELSON, S. B., TOTH, L. J., AND SUR, M. Effect of stimulus contrast and size on NMDA receptor activity in cat lateral geniculate nucleus. *J. Neurophysiol.* 68: 182–196, 1992.

LEDOUX, J. E., RUGGIERO, D. A., AND REIS, D. J. Projections to the subcortical forebrain from anatomically defined regions of the medial geniculate body in the rat. *J. Comp. Neurol.* 242: 182–213, 1985.

LUND, J. S., LUND, R. D., HENDRICKSON, A. E., BUNT, A. H., AND FUCHS, A. F. The origin of efferent pathways from the primary visual cortex, area 17, of the macaque monkey as shown by retrograde transport of horseradish peroxidase. *J. Comp. Neurol.* 164: 287–303, 1975.

LUTHI, A. AND MCCORMICK, D. A. Periodicity of thalamic synchronized oscillations: the role of Ca^{2+}-mediated upregulation of I_h. *Neuron* 20: 553–563, 1998.

MAJOROSSY, K. AND KISS, A. Specific patterns of neuron arrangement and of synaptic articulation in the medial geniculate body. *Exp. Brain Res.* 26: 1–17, 1976.

MAJOROSSY, K. AND RETHELYI, M. Synaptic architecture in the medial geniculate body (ventral division). *Exp. Brain Res.* 6: 306–323, 1968.

MALMIERCA, M. S., REES, A., AND LEBEAU, F.E.N. Ascending projections to the medial geniculate body from physiologically identified loci in the inferior colliculus. In: *Acoustical Signal Processing in the Central Auditory System*, edited by J. Syka. New York: Plenum Press, 1997, p. 295–302.

MCCORMICK, D. A. Functional properties of a slowly inactivating potassium current in guinea pig dorsal lateral geniculate relay neurons. *J. Neurophysiol.* 66: 1176–1189, 1991.

MCCORMICK, D. A. Neurotransmitter actions in the thalamus and cerebral cortex and their role in neuromodulation of thalamocortical activity. *Prog. Neurobiol.* 39: 337–398, 1992.

McCormick, D. A. and Bal, T. Sensory gating mechanisms of the thalamus. *Curr. Opin. Neurobiol.* 4: 550–556, 1994.

McCormick, D. A. and Pape, H. C. Properties of a hyperpolarization-activated cation current and its role in rhythmic oscillation in thalamic relay neurones. *J. Physiol. (Lond.)* 431: 291–318, 1990a.

McCormick, D. A. and Pape, H. C. Noradrenergic and serotonergic modulation of a hyperpolarization-activated cation current in thalamic relay neurones. *J. Physiol. (Lond.)* 431: 319–342, 1990b.

Mitani, A., Itoh, K., and Mizuno, N. Distribution and size of thalamic neurons projecting to layer I of the auditory cortical fields of the cat compared to those projecting to layer IV. *J. Comp. Neurol.* 257: 105–121, 1987.

Montero, V. M. Ultrastructural identification of axon terminals from the thalamic reticular nucleus in the medial geniculate body in the rat: an EM autoradiographic study. *Exp. Brain Res.* 51: 338–342, 1983.

Monyer, H., Burnashev, N., Laurie, D. J., Sakmann, B., and Seeburg, P. H. Developmental and regional expression in the rat brain and functional properties of four NMDA receptors. *Neuron* 12: 529–540, 1994.

Mooney, D. M., Hu, B., and Senatorov, V. V. Muscarine induces an anomalous inhibition of synaptic transmission in rat auditory thalamic neurons in vitro. *J. Pharmacol. Exp. Ther.* 275: 838–844, 1995.

Morest, D. K. The neuronal architecture of the medial geniculate body of the cat. *J. Anat.* 98: 611–630, 1964.

Morest, D. K. The laminar structure of the medial geniculate body of the cat. *J. Anat.* 99: 143–160, 1965a.

Morest, D. K. The lateral tegmental system of the midbrain and the medial geniculate body: study with Golgi and Nauta methods in the cat. *J. Anat.* 99: 611–634, 1965b.

Nelson, P. G. and Erulkar, S. D. Synaptic mechanisms of excitation and inhibition in the central auditory pathway. *J. Neurophysiol.* 26: 908–923, 1963.

Ohara, P. T. and Havton, L. A. Dendritic architecture of rat somatosensory thalamorcortical projection neurons. *J. Comp. Neurol.* 341: 159–171, 1994.

Ojima, H. Terminal morphology and distribution of corticothalamic fibers originating from layers 5 and 6 of cat primary auditory cortex. *Cereb. Cortex* 4: 646–663, 1994.

Pallas, S. L. and Sur, M. Morphology of retinal axon arbors induced to arborize in a novel target, the medial geniculate nucleus. II. Comparison with axons from the inferior colliculus. *J. Comp. Neurol.* 349: 363–376, 1994.

Pape, H. C. and McCormick, D. A. Noradrenaline and serotonin selectively modulate thalamic burst firing by enhancing a hyperpolarization-activated cation current. *Nature* 340: 715–718, 1989.

Pape, H. C. and McCormick, D. A. Electrophysiological and pharmacological properties of interneurons in the cat dorsal lateral geniculate nucleus. *Neuroscience* 68: 1105–1125, 1995.

Pare, D., Dossi, R. C., and Steriade, M. Three types of inhibitory postsynaptic potentials generated by interneurons in the anterior thalamic complex of cat. *J. Neurophysiol.* 66: 1190–1204, 1991.

Paxinos, G. and Watson, C. *The Rat Brain in Stereotaxic Coordinates.* San Diego: Academic Press, 1986.

Peruzzi, D., Bartlett, E., Smith, P. H., and Oliver, D. L. A monosynaptic GABAergic input from the inferior colliculus to the medial geniculate body in rat. *J. Neurosci.* 17: 3766–3777, 1997.

Rouiller, E. M., Colomb, E., Capt, M., and de Ribaupierre, F. Projections of the reticular complex of the thalamus onto physiologically characterized regions of the medial geniculate body. *Neurosci. Let.* 53: 227–232, 1985.

Rouiller, E. M. and de Ribaupierre, F. Origin of afferents to physiologically defined regions of the medial geniculate body of the cat: ventral and dorsal divisions. *Hear. Res.* 19: 97–114, 1985.

Rouiller, E. M. and Welker, E. Morphology of corticothalamic terminals arising from the auditory cortex of the rat: a Phaseolus vulgaris-leucoagglutinin (PHA-L) tracing study. *Hear. Res.* 56: 179–190, 1991.

Ryugo, D. K. and Weinberger, N. M. Corticofugal modulation of the medial geniculate body. *Exp. Neurol.* 51: 377–391, 1976.

St. Marie, R. L., Stanforth, D. A., and Jubelier, E. M. Substrate for rapid feedforward inhibition of the auditory forebrain. *Brain Res.* 765: 173–176, 1997.

Senatorov, V. V., Mooney, D., and Hu, B. The electrogenic effects of Na(+)-K(+)-ATPase in rat auditory thalamus. *J. Physiol.* 502: 375–385, 1997.

Senatorov, V. V. and Hu, B. Differential Na(+)-K(+)-ATPase activity in rat lemniscal and non-lemniscal auditory thalami. *J. Physiol. (Lond.)* 502: 387–395, 1997.

Shosaku, A. and Sumitomo, I. Auditory neurons in the rat thalamic reticular nucleus. *Exp. Brain Res.* 49: 432–442, 1983.

Smith, P. H. Anatomy and physiology of multipolar cells in the rat inferior collicular cortex using the in vitro brain slice technique. *J. Neurosci.* 12: 3700–3715, 1992.

Steriade, M. Synchronized activities of coupled oscillators in the cerebral cortex and thalamus at different levels of vigilance. *Cereb. Cortex* 7: 583–604, 1997.

Steriade, M., Timofeev, I., Durmuller, N., and Grenier, F. Dynamic properties of corticothalamic neurons and local cortical interneurons generating fast rhythmic (30–40 Hz) spike bursts. *J. Neurophysiol.* 79: 483–490, 1998.

Suga, N., Zhang, Y., and Yan, J. Sharpening of frequency tuning by inhibition in the thalamic auditory nucleus of the mustached bat. *J. Neurophysiol.* 77: 2098–2114, 1997.

Tennigkeit, F., Schwarz, D. W., and Puil, E. Mechanisms for signal transformation in lemniscal auditory thalamus. *J. Neurophysiol.* 76: 3597–3608, 1996.

Tennigkeit, F., Schwarz, D. W., and Puil, E. Modulation of bursts and high-threshold calcium spikes in neurons of rat auditory thalamus. *Neuroscience* 83: 1063–1073, 1998.

Turner, J. P., Anderson, C. M., Williams, S. R., and Crunelli, V. Morphology and membrane properties of neurones in the cat ventrobasal thalamus in vitro. *J. Physiol. (Lond.)* 505: 707–726, 1997.

Turner, J. P., Leresche, N., Guyon, A., Soltesz, I., and Crunelli, V. Sensory input and burst firing output of rat and cat thalamocortical cells: the role of NMDA and non-NMDA receptors. *J. Physiol. (Lond.)* 480: 281–295, 1994.

Warren, R. A., Agmon, A., and Jones, E. G. Oscillatory synaptic interactions between ventroposterior and reticular neurons in mouse thalamus in vitro. *J. Neurophysiol.* 72: 1993–2003, 1994.

Wenzel, A., Fritschy, J. M., Mohler, H., and Benke, D. NMDA receptor heterogeneity during postnatal development of the rat brain: differential expression of the NR2A, NR2B, and NR2C subunit proteins. *J. Neurochem.* 68: 469–478, 1997.

Wenzel, A., Scheurer, L., Kunzi, R., Fritschy, J. M., Mohler, H., and Benke, D. Distribution of NMDA receptor subunit proteins NR2A, 2B, 2C and 2D in rat brain. *Neuroreport* 7: 45–48, 1995.

Winer, J. A. The functional architecture of the medial geniculate body and the primary auditory cortex. In: *The Mammalian Auditory Pathway: Neuroanatomy*, edited by R. R. Fay, A. N. Popper and D. B. Webster. New York: Springer-Verlag, 1992, p. 222–409.

Winer, J. A. and Larue, D. T. Anatomy of glutamic acid decarboxylase immunoreactive neurons and axons in the rat medial geniculate body [published erratum appears in *J. Comp. Neurol.* 280: 499–500, 1989]. *J. Comp. Neurol.* 278: 47–68, 1988.

Winer, J. A. and Morest, D. K. Axons of the dorsal division of the medial geniculate body of the cat: a study with the rapid Golgi method. *J. Comp. Neurol.* 224: 344–370, 1984.

Winer, J. A. and Morest, D. K. The neuronal architecture of the dorsal division of the medial geniculate body of the cat. A study with the rapid Golgi method. *J. Comp. Neurol.* 221: 1–30, 1983.

Winer, J. A., Saint Marie, R. L., Larue, D. T., and Oliver, D. L. GABAergic feedforward projections from the inferior colliculus to the medial geniculate body. *Proc. Natl. Acad. Sci. USA* 93: 8005–8010, 1996.

Yan, J. and Suga, N. Corticofugal modulation of time-domain processing of biosonar information in bats. *Science* 273: 1100–1103, 1996.

Zhang, Y. and Suga, N. Corticofugal amplification of subcortical responses to single tone stimuli in the mustached bat. *J. Neurophysiol.* 78: 3489–3492, 1997.

Zhang, Y., Suga, N., and Yan, J. Corticofugal modulation of frequency processing in bat auditory system. *Nature* 387: 900–903, 1997.